


## Burst properties of the most recurring transient magnetar SGR J1935+2154

LIN LIN <sup>1</sup>, ERSIN GÖĞÜŞ,<sup>2</sup> OLIVER J. ROBERTS,<sup>3</sup> CHRYSSA KOUVELIOTOU,<sup>4,5</sup> YUKI KANEKO,<sup>2</sup>  
ALEXANDER J. VAN DER HORST,<sup>4,5</sup> AND GEORGE YOUNES<sup>4,5</sup>

<sup>1</sup>*Department of Astronomy, Beijing Normal University, Beijing 100875, China*

<sup>2</sup>*Sabancı University, Faculty of Engineering and Natural Sciences, İstanbul 34956 Turkey*

<sup>3</sup>*Universities Space Research Association, 320 Sparkman Drive, Huntsville, AL 35805, USA*

<sup>4</sup>*Department of Physics, The George Washington University, 725 21st Street NW, Washington, DC 20052, USA*

<sup>5</sup>*Astronomy, Physics, and Statistics Institute of Sciences (APSIS), The George Washington University, Washington, DC 20052, USA*

(Received July 14, 2020; Revised July 14, 2020; Accepted July 14, 2020)

Submitted to ApJ

### ABSTRACT

We present timing and time-integrated spectral analysis of 127 bursts from SGR J1935+2154. These bursts were observed with the Gamma-ray Burst Monitor on the *Fermi Gamma-ray Space Telescope* and the Burst Alert Telescope on the *Neil Gehrels Swift Observatory* during the source's four active episodes from 2014 to 2016. This activation frequency makes SGR J1935+2154 the most burst prolific transient magnetar. We find the average duration of all the detected bursts to be much shorter than the typical, anticipated value. We fit the burst time-integrated spectra with two black-body functions, a Comptonized model and three other simpler models. Bursts from SGR J1935+2154 exhibit similar spectral properties to other magnetars, with the exception of the power law index from the Comptonized model, which correlates with burst fluence. We find that the durations and both black-body temperatures of the bursts have significantly evolved across the four active episodes. We also find that the burst time history exhibits two trends, which are strongly correlated with the decay of the persistent emission in each outburst.

*Keywords:* soft gamma repeater: general — soft gamma repeater: individual  
(SGR J1935+2154)

### 1. INTRODUCTION

Magnetars comprise a group of isolated neutron stars with extremely strong magnetic fields (Kouveliotou et al. 1998), which fully determine the emission properties of these systems. Magnetars slow down rapidly ( $\dot{P} \sim 10^{-13} - 10^{-11} \text{ s s}^{-1}$ ) likely under the influence of large magnetic torques. As a

result, their rotational periods are very slow ( $P \sim 2 - 12$  s), even though they are young objects, typically  $10^3$  years old. Recently, magnetar-like activity was detected from the central compact object of supernova remnant, RCS 103. With a rotational period of 6.67 hrs, it may be the longest of any observed magnetar to-date (Rea et al. 2016; D’Ài et al. 2016). The typical X-ray luminosity of a magnetar ranges between  $10^{33} - 10^{36}$  erg s $^{-1}$ , which exceeds their rotational energy losses by a few orders of magnitude. Consequently, it has been suggested that the X-ray emission in magnetars is powered by the decay of their extreme magnetic fields ( $B \sim 10^{14} - 10^{15}$  G). However, two sources were discovered in the last decade with relatively low inferred dipole fields, of the order of  $B \sim 10^{12}$  G (Rea et al. 2010, 2012, 2014; An, & Archibald 2019). The spectral properties of these two sources suggest that their surface magnetic field is still comparable to those of the magnetar population, albeit, with a more complicated configuration than a simple dipole field (Güver et al. 2011; Tiengo et al. 2013).

The majority of magnetars undergo occasional random outbursts during which time, their persistent emission increases significantly while simultaneously emitting bursts (or intermediate flares), in the hard X-ray or soft  $\gamma$ -ray energy regime. So far, we have detected bursts from 18 out of 23 confirmed magnetars (Olausen, & Kaspi 2014). Based on their duration and peak luminosities, magnetar bursts can be classified into three types. Giant Flares, which are the rarest and most energetic magnetar events. Only three of this kind have been observed, from three different sources (Mazets et al. 1979; Hurley et al. 1999, 2005; Palmer et al. 2005). All three events start with an initial hard peak lasting 0.1 – 0.2 s with a luminosity of  $10^{44} - 10^{47}$  erg s $^{-1}$ , followed by a spin-period-modulated soft tail, lasting hundreds of seconds. Intermediate flares last 1 – 40 s and have peak luminosities of  $10^{41} - 10^{43}$  erg s $^{-1}$ . The most common events are short bursts, with a typical duration of  $\sim 0.1$  s and peak luminosities of  $10^{39} - 10^{41}$  erg s $^{-1}$ . Bursts and flares are also powered by the magnetic field, either through neutron star crustquakes (Thompson, & Duncan 1995) or via magnetic field line reconnection (Lyutikov 2003). For a recent magnetar burst review, see Turolla et al. (2015).

During an outburst, the persistent X-ray luminosity of the source may increase at a rate 10 – 1000 times its quiescent level. The flux then gradually decays back to a pre-outburst level on timescales from weeks to years (Rea, & Esposito 2011; Coti Zelati et al. 2018). Almost all magnetar observed outbursts are accompanied by the detection of bursting activity. However, there is no unique source activation trend. For example, Magnetar 1E 1841 – 045 showed no obvious change in its persistent X-ray emission after emitting short bursts (Lin et al. 2011b). Conversely, there are transient magnetars that have remarkable increases in their persistent X-ray flux after their bursting episode(s).

SGR J1935+2154 was discovered after emitting a short burst which triggered the Burst Alert Telescope (BAT) aboard the *Neil Gehrels Swift Observatory* (hereafter *Swift*), on 2014 July 5. Follow-up observations carried out between July, 2014 and March, 2015 with *Chandra* and *XMM-Newton* allowed the measurement of its spin period and spin-down rate, found to be  $P = 3.24$  s and  $\dot{P} = 1.43(1) \times 10^{-11}$  s s $^{-1}$ , respectively. This implies a dipole-magnetic field of  $B \sim 2.2 \times 10^{14}$  G (Israel et al. 2016), confirming its magnetar nature. Since its discovery, SGR J1935+2154 exhibited burst active episodes almost annually, becoming the most recurring transient magnetar ever observed. Kozlova et al. (2016) reported an intermediate flare from SGR J1935+2154 detected by four Interplanetary network (IPN) spacecraft on April 12<sup>th</sup> 2015 (not observed by the Gamma-ray Burst Monitor (GBM) aboard *Fermi*). The flare lasted for  $\sim 1.7$  s with an energy fluence of  $\sim 2.5 \times 10^{-5}$  erg cm $^{-2}$ . The source went into outburst in 2014 (Israel et al. 2016), 2015, and twice in 2016. During the

**Table 1.** *Swift*/BAT SGR J1935+2154 bursts.

Observational ID	Date	Number of Bursts
00603488000	2014-07-05	3
00632158000	2015-02-22	1
00632159000	2015-02-22	1
00686443000	2016-05-16	1
00686761000	2016-05-18	2
00686842000	2016-05-19	1
00687123000	2016-05-21	3
00687124000	2016-05-21	3
00701182000	2016-06-23	4
00701590000	2016-06-26	2

2015 outburst, a hard X-ray spectral component was revealed in the persistent source spectrum with *NuSTAR* observations. During the 2016 outbursts, the soft X-ray flux was found to have increased by about 7 times the previous reported levels (Younes et al. 2017).

We report the results of our extensive search for short bursts from this prolific transient magnetar, using a Bayesian block method to search the *Swift*/BAT and *Fermi*/GBM data. We performed detailed temporal and spectral analyses on all identified short bursts to establish not only their collective statistical properties, but any characteristic variations during each burst-active episode. The layout of our study is as follows: The data reduction and burst search procedure are introduced in Section 2. In Section 3, we present the detailed spectral and temporal analyses for all reported bursts, including their lightcurves and localization. We discuss our results in Section 4.

## 2. OBSERVATIONS AND BURST SAMPLE

The *Swift*/BAT is a sensitive, mask-coded imaging instrument with a 1.4 steradian partially coded field of view (FoV) in the 15 – 150 keV energy band (Barthelmy et al. 2005). Nominally, BAT works in a surveying mode, which only provides detector plan histograms integrated for about five minutes. When the instrument is triggered by a burst, it shifts to a burst mode, and the time tagged event list is restored. This event list covers a time interval of about  $-200$  to  $2000$  s either side of the trigger time, with a time resolution of  $\sim 0.2$  ms. Considering that most magnetar bursts are short, we only study the time-tagged event list data. BAT was triggered 10 times by SGR J1935+2154 bursts between 2014 and 2016. Their observational IDs are listed in Table 1.

The *Fermi*/GBM comprises 12 NaI(Tl) detectors ( $\sim 8$  keV – 1 MeV), each with a diameter of 12.7 cm and length of 1.27 cm. The detectors are located in clusters of three at each of the four corners of the spacecraft (Meegan et al. 2009). GBM also has two BGO detectors on opposing sides of the spacecraft, however they are not used in this analysis as the spectral range of the magnetars reported in this study lie below their effective energy range (0.2–40 MeV). As an all-sky monitor, GBM has an unocculted FoV of 8 steradians. Since 2012, GBM data are recorded in the continuous time-tagged event (TTE) mode with a fine temporal resolution of  $2 \mu\text{s}$ . The spectral resolution comprises 128 pseudo-logarithmically scaled channels over an energy range of 8 – 1000 keV. These

data types and its monitoring nature make GBM ideal for Magnetar burst studies. GBM was triggered 62 times by bursts from SGR J1935+2154 from 2014 – 2016.

Not all Magnetar bursts triggered both BAT and GBM, even when the source was within the FoV of both instruments. Due to the triggering settings of GBM, new bursts that occur five minutes after a previous trigger, or weak bursts below the trigger thresholds, are usually not picked up. In addition to GBM being unable to trigger five minutes following a burst trigger, the thresholds on the BAT are increased for re-triggering on a known source. An un-triggered search for bursts through the entire available data is therefore essential in order to have a burst history that is as complete as possible for any magnetar source.

The Bayesian block method is a non-parametric modeling technique for detecting and characterizing local variability in time-series data (Scargle et al. 2013). The automated process divides the binned lightcurve or time-tagged event list into blocks, each block being consistent with a constant rate. It then finds the optimal segmentation or boundaries between the blocks by maximizing likelihood, termed change points. These step functions have no priors in amplitude nor duration. This method has been used in standard BAT data analysis procedures to calculate the duration of Gamma-Ray Bursts (GRBs), especially in helping identify the extended emission following some short GRBs (Norris et al. 2010; Kaneko et al. 2015). Lin et al. (2013) applied this method to identify weak bursts in *XMM-Newton* and *Swift*/X-ray Telescope (XRT) observations of two magnetars and found the properties of those bursts to be dimmer by 1 – 2 orders of magnitude than the triggered ones.

We performed the un-triggered burst search using the Bayesian block method on the BAT triggered-event data and GBM continuous TTE data. For the BAT data, we first extracted the mask-weighted lightcurve over the 15 – 150 keV band with 4 ms temporal resolution for each trigger. We then searched through the lightcurves using the same two-step procedure described in Gögüş et al. (2016). We found 11 additional events in the 10 BAT triggered event data sets. The number of bursts found in each observation is listed in Table 1. For each BAT burst we extracted the spectrum using *batbinevt*, made required corrections (*batupdatephakw* and *batphasyserr*), and generated responses (*batdrngen*). We then performed time-integrated spectral analysis with variable bin-sizes of at least  $1\sigma$  significance, using *XSpec* (Arnaud 1996) and  $\chi^2$  statistics.

We also performed the Bayesian block search over the continuous TTE GBM data for the following time intervals: July 1<sup>st</sup> – 15<sup>th</sup>, 2014; February 15<sup>th</sup> – April 15<sup>th</sup>, 2015; and January 1<sup>st</sup> – October 31<sup>st</sup>, 2016. The search procedure is similar to what we used in Lin et al. (2013), with some modifications to the parameters. In order to limit computation time, we rebinned the TTE data over an energy range of 10 – 100 keV into 8 ms. We then started a two-round search using a timing window of 8 s. We repeated the same search for all 12 NaI(Tl) detectors, flagging simultaneous events detected in two or more detectors. Detectors with an angle to the source of less than  $60^\circ$ <sup>1</sup>, without any blockage by the satellite were then chosen and their location was calculated on the sky. We found 112 SGR J1935+2154 bursts in the GBM data, including 62 triggered events. Overall, there are 127 unique bursts from SGR J1935+2154 observed with BAT and GBM, with six events simultaneously recorded by both instruments. The ID, instrument information, and burst start time for all 127 bursts are listed in Table 4. We performed a spectral fit to each of these bursts with the standard

<sup>1</sup> Results do not change significantly when choosing a smaller angle, e.g.,  $40^\circ$

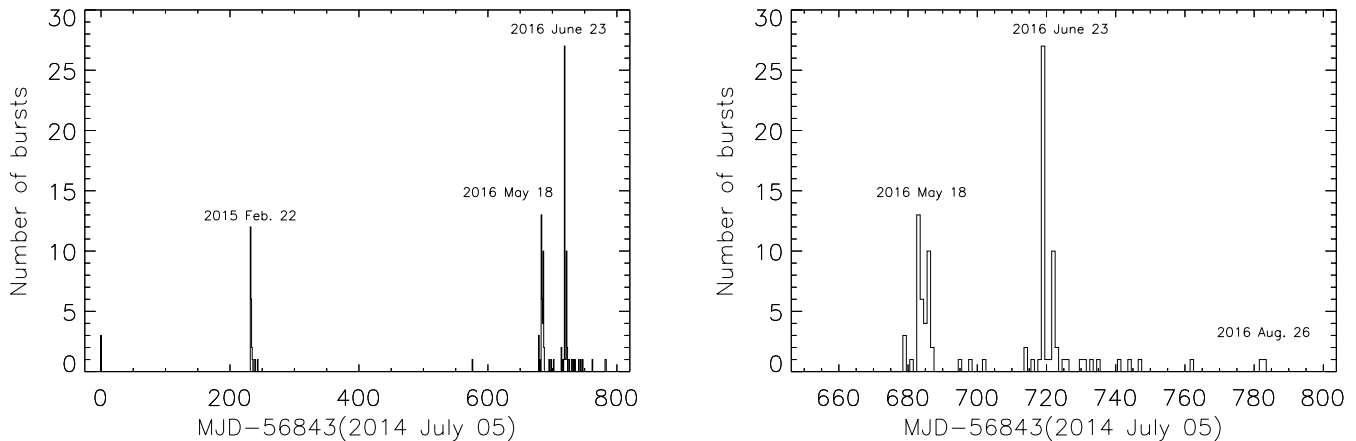


**Figure 1.** The burst time history of SGR J1935+2154 in 1-day time bins. *Left:* The burst history from July, 2014 - August, 2016. *Right:* The expanded burst history starting from May, 2016.

**Table 2.** SGR J1935+2154 Activation Intervals.

Episode	Start date	End date	in BAT/GBM/Both	Total Number	Burst fluence <sup>†</sup> ( $10^{-7}$ erg $\text{cm}^{-2}$ )	Burst energy <sup>*,†</sup> ( $10^{39}$ erg)
1	2014-07-05	2014-07-05	1 / 0 / 2	3	1.1	1.1
2	2015-02-22	2015-03-05	2 / 22 / 0	24	41.4	40.1
3	2016-05-14	2016-06-06	6 / 33 / 3	42	119.5	115.8
4	2016-06-18	2016-07-21	5 / 48 / 1	54	456.1	442.0

NOTE—\* Assuming a distance of 9 kpc to SGR J1935+2154.

<sup>†</sup> Values are the sum of both the burst fluence and the burst energy for all bursts in each episode.

GBM analysis software *RMFIT* using Castor C-statistics (*c-stat*). The detector response matrices were generated with *GBMDRM v2.0*.

### 3. RESULTS

#### 3.1. Burst activity history

We define an active bursting episode as the time period during which more than two bursts are emitted, with no bursts observed 10 days either side of this range. Using this definition, we find four bursting episodes for SGR J1935+2154. We exhibit the source burst history in Figure 1 and summarize the four episode properties in Table 2. SGR J1935+2154 became increasingly active in 2015 and 2016. It ceased activity after August, 2016. We notice that at least ten bursts were detected within one day for all active burst episodes, except for 2014. Considering the persistent flux increase following each episode (Younes et al. 2017), SGR J1935+2154 should be classified as a prolific transient in the scheme of Göğüş (2014).

Aside from these bursting episodes, we found four isolated events with burst IDs of 28, 125, 126 and 127)<sup>2</sup>. We also searched seven days either side of the intermediate flare that occurred on the 12<sup>th</sup> of April 2015, but found no other bursts.

### 3.2. Burst localization

As an imaging instrument, the BAT has the capability to locate each triggered burst to within an uncertainty of several arcminutes. We search for bursts in the mask-weighted lightcurves that trace back to the position of SGR J1935+2154, considering all additional short events to also originate from the source (not statistical fluctuations). The false positive rate of a change point (a block containing two change points), was set to 5 % during the search process, using the data and prior number of change points. The algorithm is defined by simulations of the pure noise (Scargle et al. 2013). We iterate the search process until no further modification to the change points is necessary and the parameters are consistent. See Scargle et al. (2013) for more details.

*Fermi*/GBM provides rough burst locations by combining the count rates in the NaI(Tl) detectors that meet the aforementioned source-angle criterion of  $\leq 60^\circ$ . The uncertainty of these locations is typically several degrees, depending on the burst peak intensity. Both triggered and un-triggered GBM events are localized with the Daughter Of Locburst (DOL) code (von Kienlin et al. 2012) using counts below 50 keV. Table 4 lists the measured locations and statistical errors at the  $1\sigma$  confidence level<sup>3</sup>. We find that the error bars presented in Table 4 and Figure 2 do not include the systematic uncertainties which are at least  $3^\circ$  (Connaughton et al. 2015). GBM Bursts located around the known position of SGR J1935+2154 (some with quite large uncertainties), are shown in Figure 2. Both the right ascension and declination values of bursts follow Gaussian distributions with the mean values close to the source position (Figure 3). While the locations of several of these bursts are consistent with SGR 1900+14 (R.A.=  $286.8^\circ$ , Dec.=  $9.3^\circ$  (Frail et al. 1999)), we find no observational evidence to suggest this source was active around the burst times presented in this study. Therefore, we consider all these events to be from SGR J1935+2154.

### 3.3. Burst durations

We select three parameters to quantify each burst duration. The Bayesian block duration ( $T_{\text{bb}}$ ) is a direct benefit from our search process, and is the total length of all Bayesian blocks for a burst event, without any artificial selection (Lin et al. 2013). We record  $T_{\text{bb}}$  for both BAT and GBM bursts.  $T_{90}$  ( $T_{50}$ ) is defined as the time interval over which the cumulative energy fluence of the burst increases from 5% (25%) to 95% (75%) of the total fluence (Kouveliotou et al. 1993). These are only calculated for the GBM bursts. The speciality of  $T_{90}$  (and  $T_{50}$ ) is that when calculating energy fluence, the response of the instrument is deconvolved. However, they may be affected by the selection (Lin et al. 2011a).

Similar to the distribution of bursts from other magnetars (Collazzi et al. 2015),  $T_{\text{bb}}$ ,  $T_{90}$  and  $T_{50}$  follow Gaussian distributions when using a logarithmic scale. We present their distributions in Figure 4. The best Gaussian fit parameters and their statistics to these burst durations are presented in Table 3. For GBM bursts,  $T_{\text{bb}}$  is generally longer than  $T_{90}$ , and the two quantities are well correlated (Figure 4). The corresponding Spearman's rank correlation coefficient is 0.85, with a

<sup>2</sup> A fourth BAT burst reported later (Cummings 2014) is not included in the sample, as the count rate data were not sufficient for further detailed analysis.

<sup>3</sup> All statistical errors of the fit parameters presented in this paper are at the  $1\sigma$  confidence level.

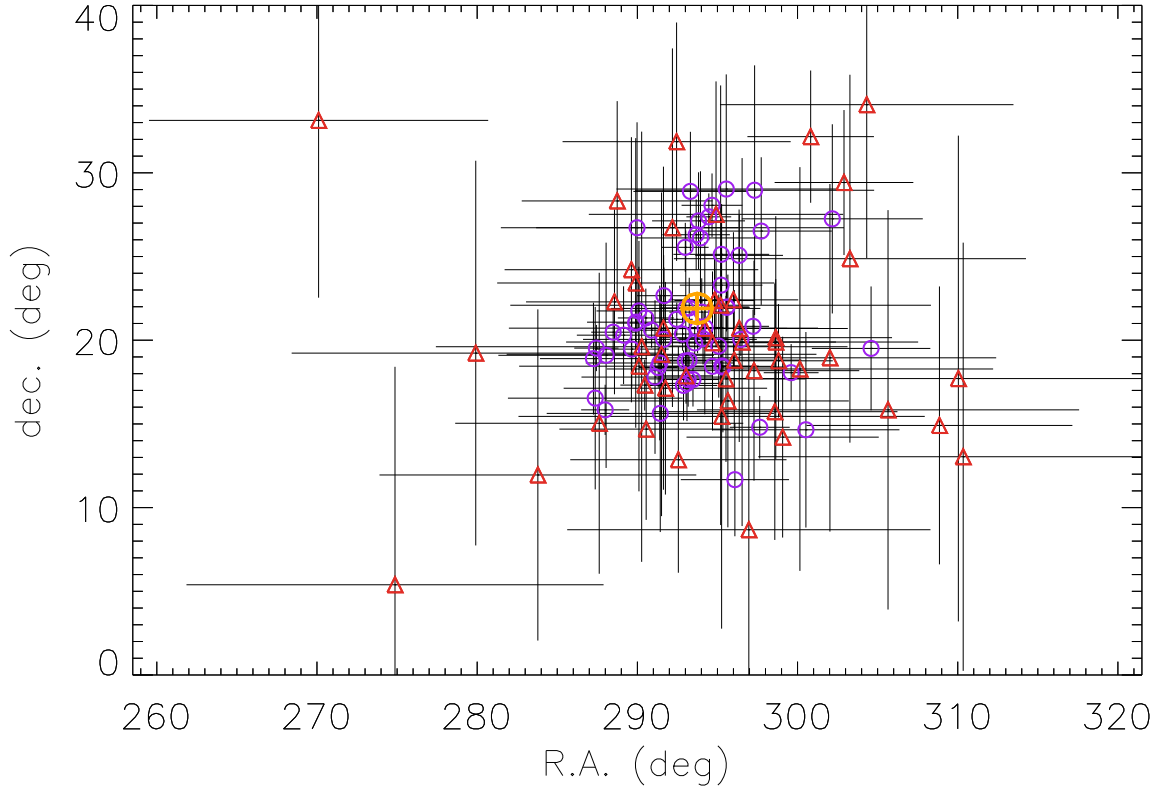


**Figure 2.** Locations of SGR J1935+2154 bursts detected with GBM. The magnetar position is marked with an orange circle with a cross. Open circles and triangles represent triggered and un-triggered bursts, respectively.

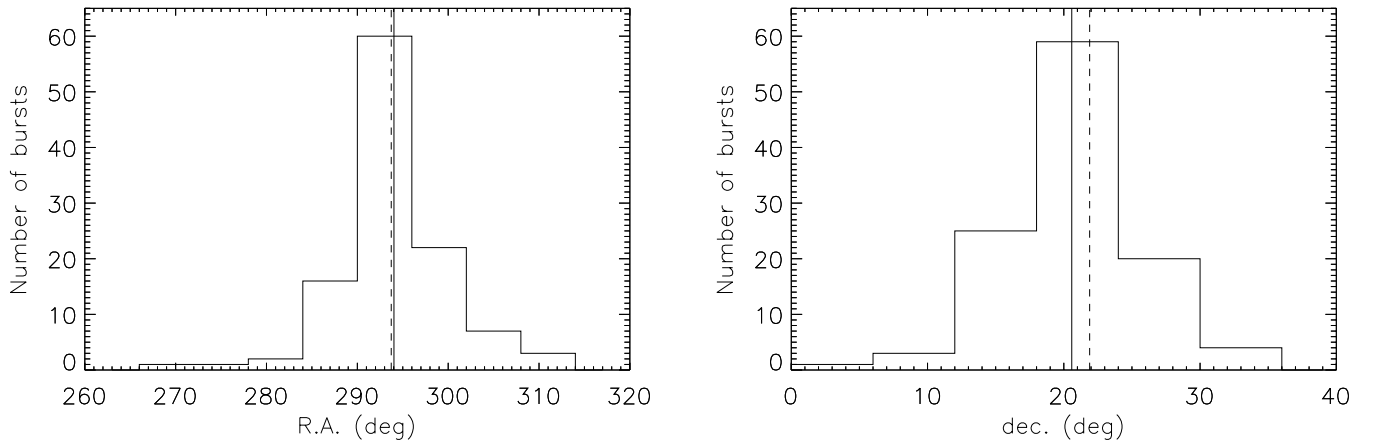


**Figure 3.** The R.A. (*left*) and Dec. (*right*) distributions for the GBM burst positions. The mean values are marked as solid lines, while the dashed lines indicate the real position of SGR J1935+2154 in each panel.

chance probability of  $5.13 \times 10^{-31}$ . A power law fit to the trend results in  $T_{90} \propto T_{\text{bb}}^{0.81 \pm 0.01}$ . A detailed list of the temporal characteristics for each burst is presented in Table 4.

### 3.4. Burst spectra

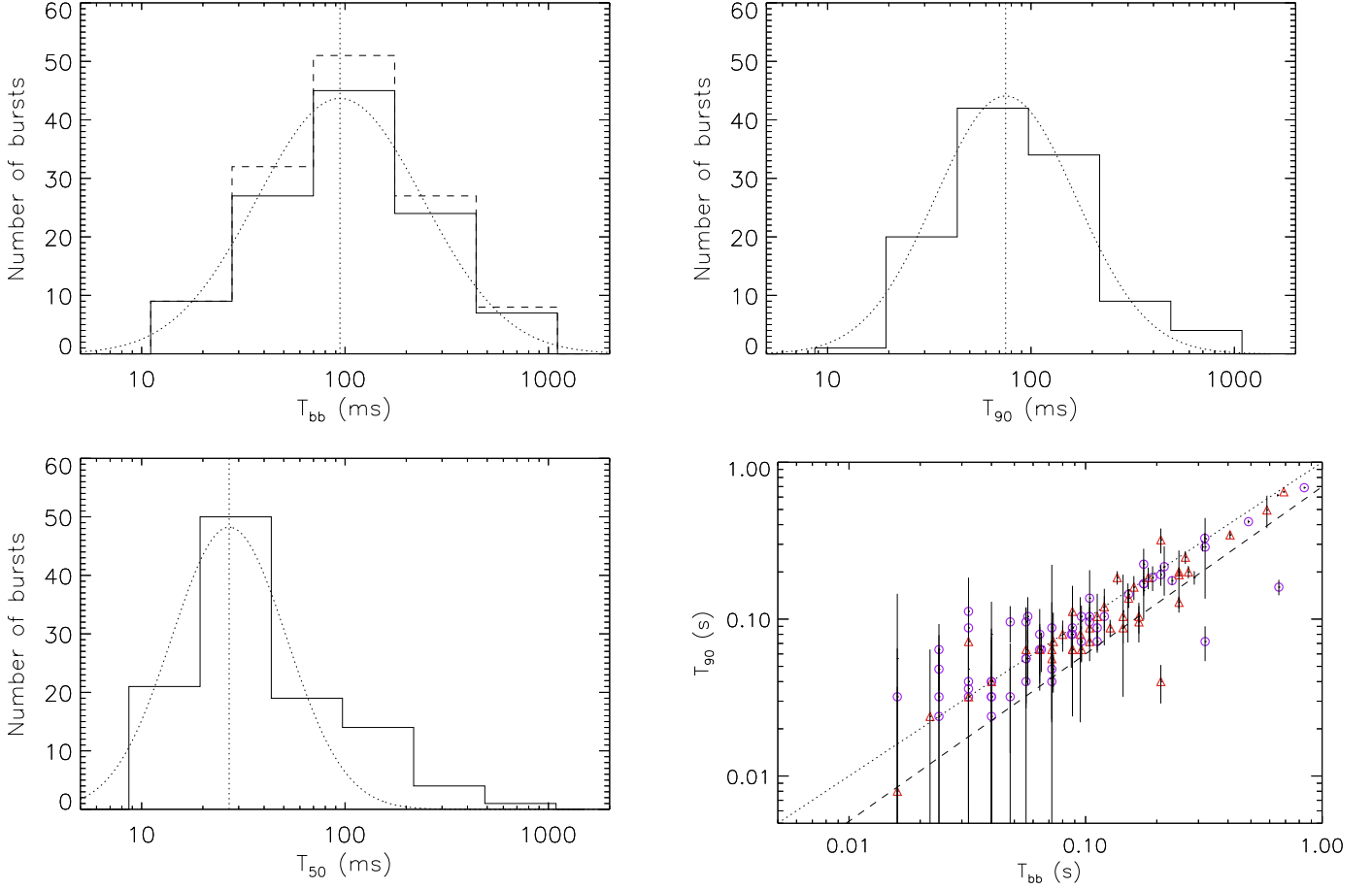


**Figure 4.** Distributions of  $T_{\text{bb}}$  (*top left*),  $T_{90}$  (*top right*) and  $T_{50}$  (*bottom left*) for the GBM bursts. The distribution of  $T_{\text{bb}}$  for *all* events is also presented in the *top left* panel with a dashed histogram. The dotted curves and lines in these three panels are the best Gaussian fits to the histograms and the mean values from the fit. The correlation between  $T_{90}$  and  $T_{\text{bb}}$  is shown in the *bottom right* panel. The purple circles and red triangles mark GBM triggered and un-triggered events, respectively. The dashed line is the best power law fit to the correlation trend and the dotted one is the  $T_{90} = T_{\text{bb}}$  line.

**Table 3.** SGR J1935+2154 Burst Duration Statistics.

Duration	Sample	Average	Gaussian fit	
		(ms)	$\mu$ (ms)	$\sigma^*$
$T_{\text{bb}}$	BAT+GBM	138	$93^{+4}_{-3}$	$0.40 \pm 0.02$
$T_{\text{bb}}$	GBM	139	$94 \pm 5$	$0.41 \pm 0.02$
$T_{90}$	GBM	123	$75 \pm 3$	$0.35 \pm 0.02$
$T_{50}$	GBM	58	$27^{+4}_{-3}$	$0.28 \pm 0.05$

NOTE—\* using a logarithmic scale



We fit the burst spectra with five models: a power law (PL), a single blackbody (BB), an optically thin thermal bremsstrahlung (OTTB), the sum of two blackbodies (BB+BB), and a PL with an exponential cutoff at higher energies (COMPT). Earlier studies found that the two complex models (BB+BB and COMPT) are preferred in describing the spectra over broad energy ranges (Israel et al. 2008; Lin et al. 2011a, 2012; van der Horst et al. 2012). The remaining three models have been traditionally used when the data cannot constrain the parameters of more complicated models. We consider a model inadequate when at least one of its parameters enters a non-physical region above a confidence level of  $1\sigma$  (e.g., a negative  $kT$  or a negative  $E_{\text{peak}}$  or normalization). Of the 127 spectra, 83 can be fit well with at least one complex model. More specifically, 36 can only be fit with a BB+BB model, and three only with COMPT. Forty-four can be fit with both BB+BB and COMPT, of which 38 resulted in a smaller  $c\text{-stat}$  (for GBM spectra) or  $\chi^2$  (for BAT spectra) when fit with a BB+BB model, and the remaining 6 when fit with a COMPT model. We note that BB+BB and COMPT are not nested models and therefore, we cannot easily compare their fit statistics. Moreover, simulation results from earlier works (Lin et al. 2011a; van der Horst et al. 2012) indicate that over an energy range of 8 – 200 keV, neither the BB+BB nor the COMPT model are preferred in terms of goodness of fit. The remaining 44 bursts, for which the complex models are inadequate, can only be fit with simpler models, such as a PL, a BB, or an OTTB model. We present the spectral parameters for all events in Table 5. In the last column of Table 4, we also include each burst fluence over 8 – 200 keV for GBM spectra, and 15 – 150 keV for BAT spectra, calculated using the spectral model with the best statistics.

Using the parameters of our BB+BB fits to 80 bursts (76 fit with GBM data and 4 fit with BAT data), we find that both low and high BB temperatures follow a Gaussian distribution with a mean value of  $4.4 \pm 0.1$  keV ( $\sigma = 1.1 \pm 0.1$  keV) and  $11.3 \pm 0.4$  keV ( $\sigma = 2.3 \pm 0.4$ ) respectively, as shown in Figure 5. These values do not change significantly if the BAT bursts are excluded. The hot BB temperature range is wider than the lower temperature one. The emission areas ( $R^2$ ), energy fluences and luminosities<sup>4</sup> of the two BB components, are strongly correlated (Figure 6). We study these correlations using only the 76 GBM bursts, as the fluxes in GBM and BAT are over different energy ranges. The Spearman rank order correlation test yields coefficients and chance probabilities of 0.8 and  $1.4 \times 10^{-19}$  for emission areas, 0.9 and  $1.9 \times 10^{-30}$  for luminosities, and 0.9 and  $1.2 \times 10^{-37}$  for fluences. Notice that the errors for these quantities are not included in the correlation test. We also fit the three correlations with a PL and find that the best fit indices are  $2.41 \pm 0.56$  for the emission areas,  $1.00 \pm 0.12$  for the luminosities, and  $1.03 \pm 0.12$  for the fluences.

We then study the distribution of the COMPT model parameters for the 45 GBM bursts (the two BAT only events are excluded from the correlation analysis due to the different energy range of the instruments). Our results are presented in Figure 7. Peak energies ( $E_{\text{peak}}$ ) range from  $\sim 25$  keV to  $\sim 40$  keV with a mean value of 31.4 keV. A Gaussian fit to the distribution gives a mean value of  $30.4 \pm 0.2$  keV and  $\sigma = 2.5 \pm 0.2$  keV. As the burst fluence increases,  $E_{\text{peak}}$  becomes slightly harder. A simple PL with an index of  $0.06 \pm 0.003$ , best fits this correlation. We note that weaker events are further from the PL fit. Similar to other Magnetars, we fit a broken PL to the data and obtain indices of  $0.06 \pm 0.001$  and  $-0.04 \pm 0.04$ . The intersection of the two PL fits is at a fluence of  $2.7 \pm 0.5 \times 10^{-7}$  erg cm<sup>-2</sup>. We also note that the index for the lower fluence bursts is weakly

<sup>4</sup> Assuming a distance to SGR J1935+2154 of 9 kpc.

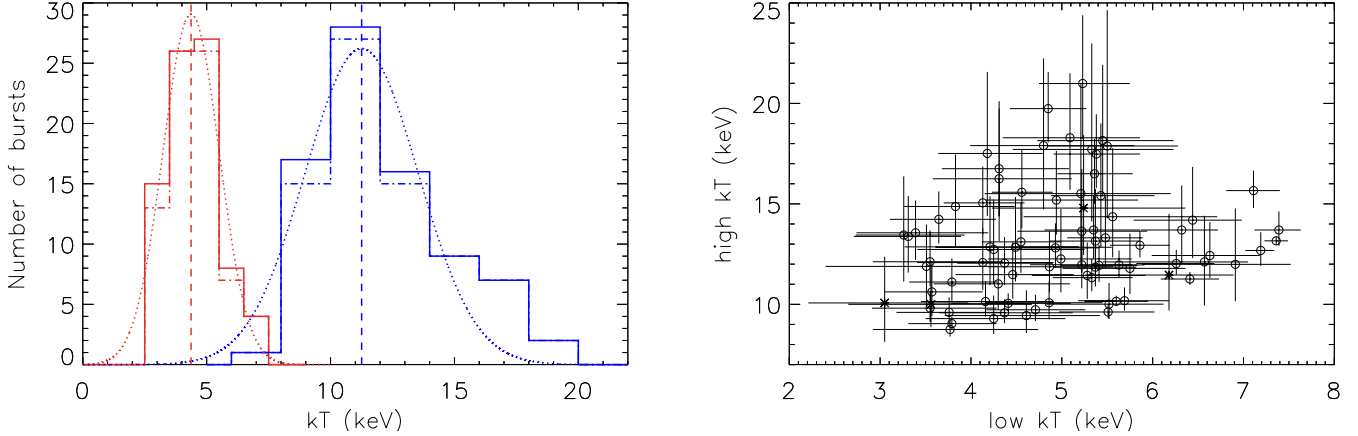


**Figure 5.** *Left:* The distribution for the two BB temperatures from the BB+BB fit. Solid and dashed-dot histograms are bursts detected with *Swift*/BAT and GBM, respectively; dotted curves are Gaussian fits to the histograms; dashed lines mark the mean fit values. The set of red lines represents the lower BB temperature ( $kT_1$ ), while the blue represents the higher BB temperature ( $kT_2$ ). *Right:* The high *v.s.* the low BB temperature. Open circles represent GBM bursts and crosses are bursts detected only with the BAT.

constrained as the break is quite close to the lowest fluence in our sample. The COMPT PL index ranges from  $-1$  to  $1$  with an average of  $0.03$ . We also fit the index distribution with a Gaussian shape, which gives a mean of  $-0.1 \pm 0.1$  with  $\sigma = 0.5 \pm 0.1$ . We find that the COMPT PL index is correlated with the fluence. The Spearman test yields a correlation coefficient of  $0.7$  with a chance probability of  $8.7 \times 10^{-9}$ . This correlation indicates that the weaker bursts have a softer spectrum.

Finally, all bursts that can only be fit with simple models are quite dim. The highest fluence among these is  $1.6 \times 10^{-7}$  erg cm $^2$ . The average temperature for 23 OTTB bursts and 9 BB bursts is  $31.2$  keV and  $9.5$  keV, respectively, and the average PL index for 12 PL bursts is  $-1.95$ .

## 4. DISCUSSION

### 4.1. Burst energetics

Since its re-emergence from quiescence, SGR J1935+2154 exhibited four active burst episodes from 2014 through late-2016. We analyzed in detail the temporal and time-integrated spectral properties of 127 short Magnetar bursts observed with the *Swift*/BAT and the *Fermi*/GBM. This sample includes events with fluences ranging from  $10^{-8}$  –  $2 \times 10^{-5}$  erg cm $^{-2}$  over an energy range of  $8$  –  $200$  keV. This range is comparable to that of other magnetars observed by GBM (e.g., SGR J1550 – 5418: van der Horst et al. (2012); Collazzi et al. (2015) and SGR J0501 + 4516: Lin et al. (2011a)). The total energy fluence emitted in our burst sample is  $6.2 \times 10^{-5}$  erg cm $^{-2}$ , corresponding to  $1.5 \times 10^{39}$  erg under the assumption of a source distance of  $9$  kpc.

In Figure 8 we present the cumulative energy fluence ( $S$ ) distribution for 112 GBM bursts from SGR J1935+2154. We fit the distribution with a broken PL. The best fits to the index for the lower and higher fluences are  $0.32 \pm 0.04$  and  $0.70 \pm 0.03$  respectively, while the break fluence is at  $7.1 \pm 0.8 \times 10^{-8}$  erg cm $^{-2}$ . The intersection of the two PL fits is much smoother than a point, which may be due to the drop-off in the detection efficiency of the instruments and the search process. In earlier studies using the GBM data, the lower cutoff in fluence was set at  $1 \times 10^{-7}$  erg cm $^{-2}$  (van der Horst et al. 2012; Collazzi et al. 2015). For comparison reasons, we select the bursts with fluences

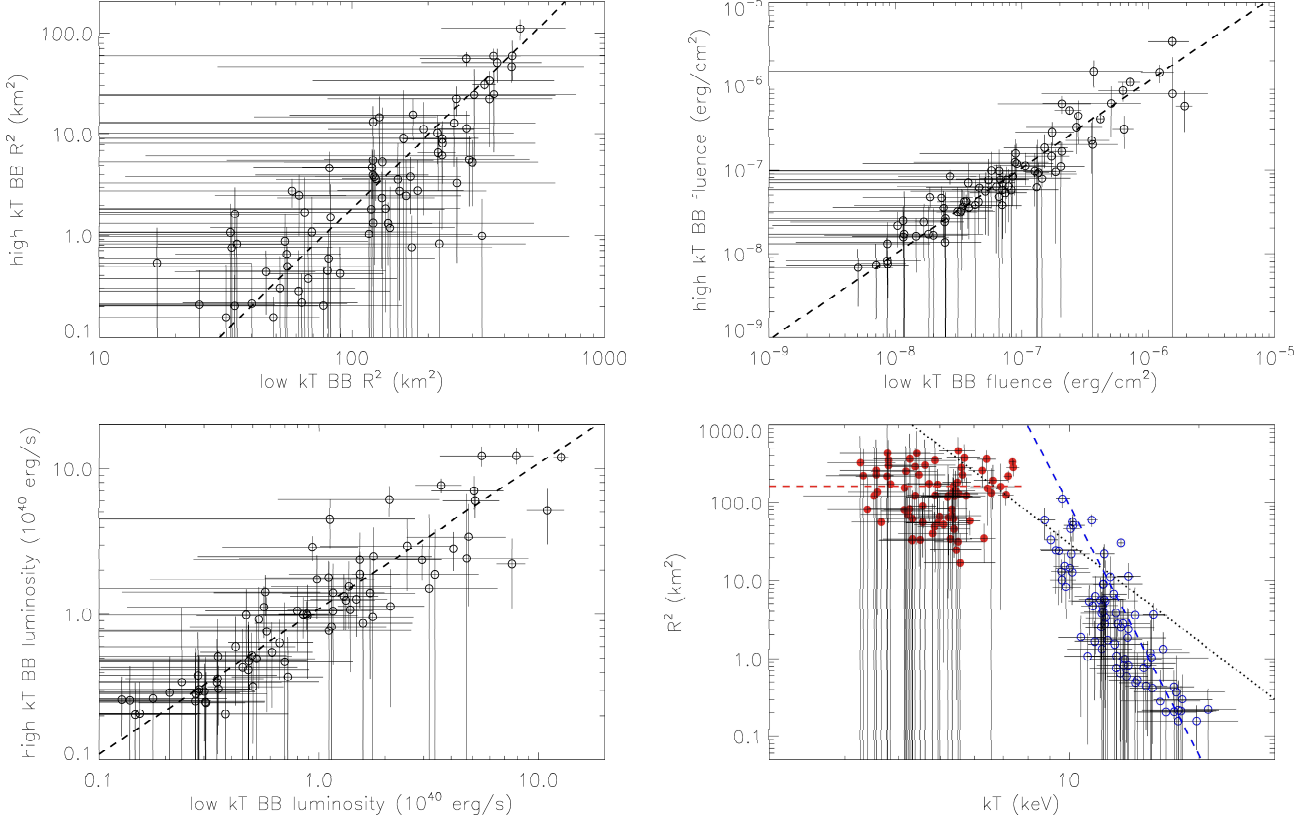


**Figure 6.** Correlations of the emission areas (*top left*), fluences (*top right*) and luminosities (*bottom left*) of the two BBs. The dashed lines are the best fit PLs for each correlation. *Bottom right*: the BB emission areas ( $R^2$ ) as a function of the two BB temperatures. The red dots and blue circles represent the cool and hot BB temperatures ( $kT_1$  and  $kT_2$ ), respectively. The blue dashed line is the PL that best fits to the hot BB component trend, while the red dashed line represents the mean value of the cool BB emission area. The dotted line is the PL that best fits both BB components.

higher than  $1 \times 10^{-7}$  erg  $\text{cm}^{-2}$ , and fit their distribution with a PL model. The index that best fits the data is  $N(> S) \propto S^{-0.78 \pm 0.01}$ , which is comparable to the value reported for other Magnetars (Cheng et al. 1996; Collazzi et al. 2015). The differential distribution of burst fluences,  $dN/dE \propto E^{-1.78}$ , is consistent with the ‘Gutenberg-Richter’ PL for earthquakes in different active regions, as pointed out by Cheng et al. (1996). The similarity between these short magnetar bursts and earthquakes supports the hypothesis that short bursts from magnetars are due to the sudden release of energy from cracks in the solid crust of neutron stars (Duncan, & Thompson 1992). We also need to keep in mind that the PL distribution is characteristic of self-organized criticality systems (Esposito et al. 2018) and exclusive properties are therefore crucial to prove the origin of short bursts.

#### 4.2. Bursts and outbursts

About 97% of our burst sample happened during four active episodes. From the first to the fourth episode, the number of bursts increased by an order of magnitude, while the energy released by these bursts increased by three orders of magnitude (Table 2). Following the onset of each episode, several X-ray instruments, such as XRT, *XMM-Newton*, *Chandra* and *NuSTAR*, observed the persistent emission outburst of SGR J1935+2154. Younes et al. (2017) performed detailed analyses from these

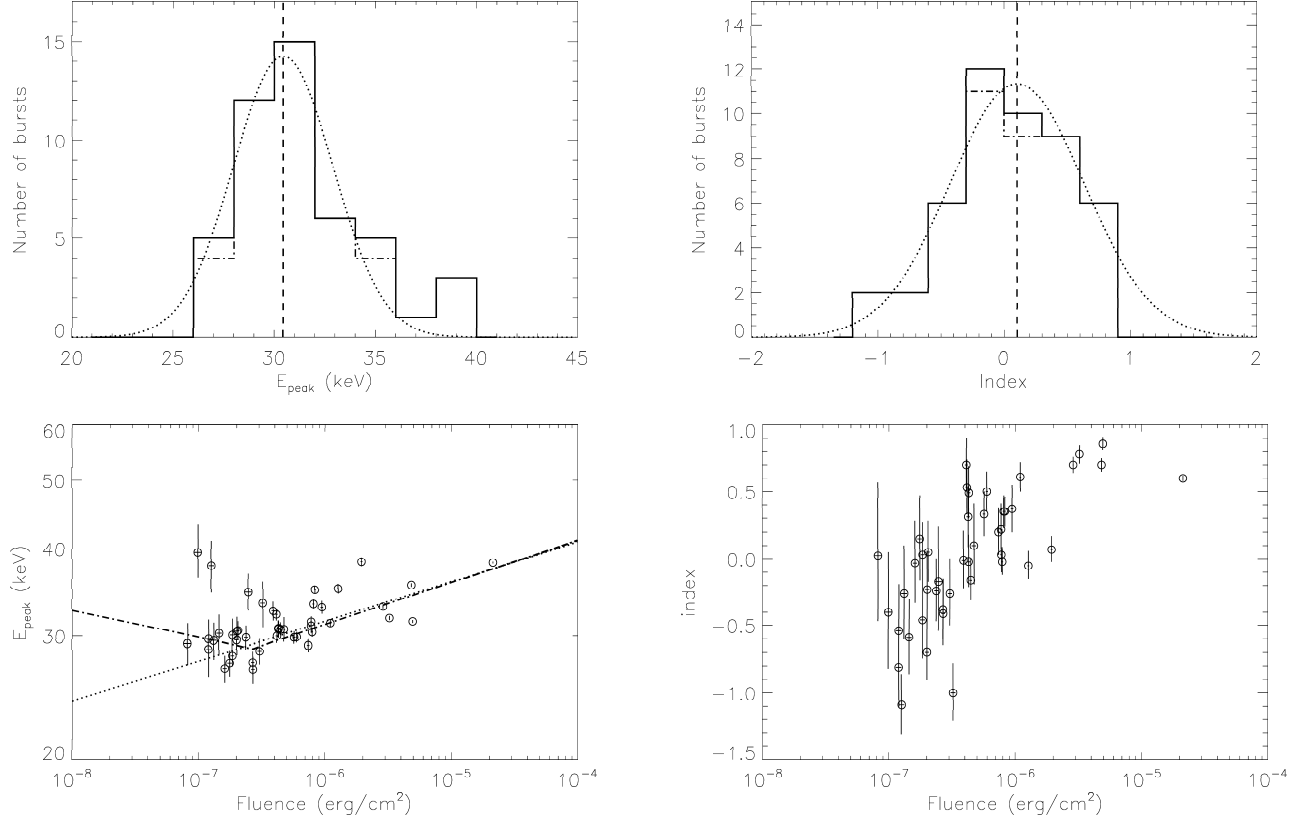


**Figure 7.** The distributions of  $E_{peak}$  (*left*) and index (*right*) of the COMPT model fits for 47 bursts (solid line) and 45 GBM bursts (dash-dotted line) are presented in the top left panel. The dotted curves are Gaussian fits to the histograms; dashed lines are mean values. In the lower panels, we show the evolution of  $E_{peak}$  (*left*) and index (*right*) as a function of fluence for the 45 GBM bursts. The best PL fit to the correlation between  $E_{peak}$  and fluence is shown as a dotted line, while the dash-dot line shows a broken PL fit to the data.

observations and concluded that the energy released in the persistent outburst of SGR J1935+2154 is roughly the same order of magnitude for all four episodes. The energy ratio between the burst and persistent emission in outbursts is  $\sim 0.03$ ,  $\sim 0.66$ ,  $\sim 5.79$  and  $\sim 12.28$  for active episodes one to four, respectively. Note that this ratio is a lower limit due to the incompleteness of the burst detection.

As a transient Magnetar, the persistent flux increase of SGR J1935+2154 is modest at the onset of each outburst (Coti Zelati et al. 2018). Its value changed by factors of 5–10, while most transient Magnetars exhibited X-ray flux increases of  $\sim 50 - 100$  at the activation onset. This increase was also usually coincident with one or more bursts. The rapid increase in X-ray flux is attributed to the cooling of a heated crustal zone at the start of the outburst (Lyubarsky et al. 2002).

We can infer from its flux increase that crustal heating takes place in SGR J1935+2154. However, as magnetar bursts are likely to radiate energy efficiently, we assume only a small fraction of energy is left to heat the crust. This could explain why the outbursts of SGR J1935+2154 are not bright at the onset, or over a longer interval. We note that this could also be linked to its recurring outburst behavior, as the source flux drops to near the quiescent flux level quickly over several months and therefore every burst reactivation would initiate a new outburst episode.

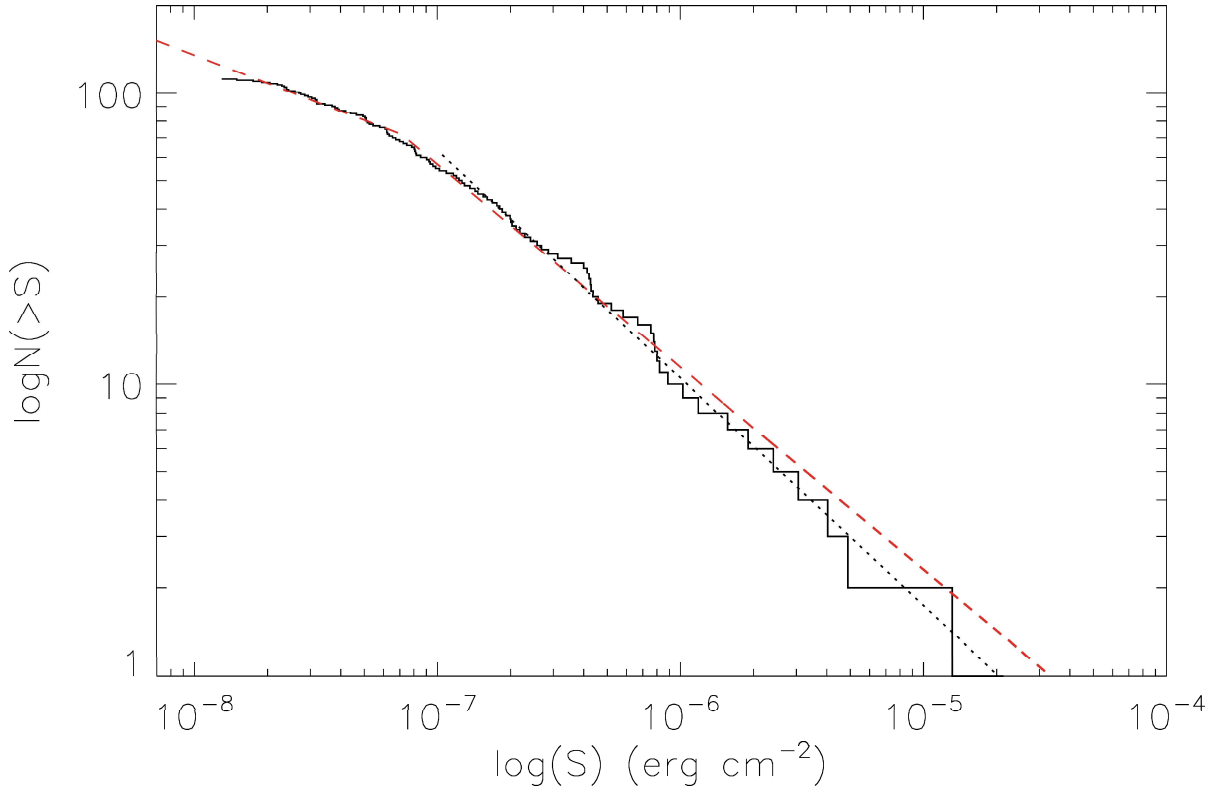


**Figure 8.** The cumulative energy fluence distribution of SGR J1935+2154 bursts. The red dashed line is the best fit of the distribution with a broken PL. The dotted line is the best PL fit to the distribution above  $1 \times 10^{-7}$  erg cm $^{-2}$ .

Younes et al. (2017) also found the increase in the average flux to be larger, decaying more rapidly in the 2016 outburst. However, the flux decay was much smoother in the first two episodes. Interestingly, we noticed that outbursts with different temporal profiles also exhibit diverse short burst history. As presented in Figure 9 and Figure 6 in Younes et al. (2017), all or the majority of bursts in the 2014 & 2015 active episodes happened on the first day of the episode, before subsequently decaying over  $\sim 100$  days. However, two episodes in 2016 started with two or three bursts, with the largest number of bursts being emitted 4 – 10 days later. The two outbursts in 2016 were brighter at the onset than those in 2014 & 2015 and quickly decayed to the quiescent level after the bursts subsided. This connection between bursts and outbursts strongly indicates that the total energy released in short bursts accelerated the fading of the persistent outburst (at least one component of the persistent emission).

#### 4.3. Comparison of burst properties during the four active episodes

A prolific transient is defined here as a magnetar emitting more than ten bursts during an active burst episode (Gögüş 2014). Prior to SGR J1935+2154, such transients included SGRs 1627–41 (Woods et al. 1999; Esposito et al. 2008), J0501+4516 (Rea et al. 2009; Gögüş et al. 2010; Lin et al. 2011a) and J1550–5418 (Israel et al. 2010; van der Horst et al. 2012; von Kienlin et al. 2012), each with only one or two burst active episodes. We reported four episodes from SGR J1935+2154 in the first three years since its discovery, making it the most prolific magnetar transient to date.

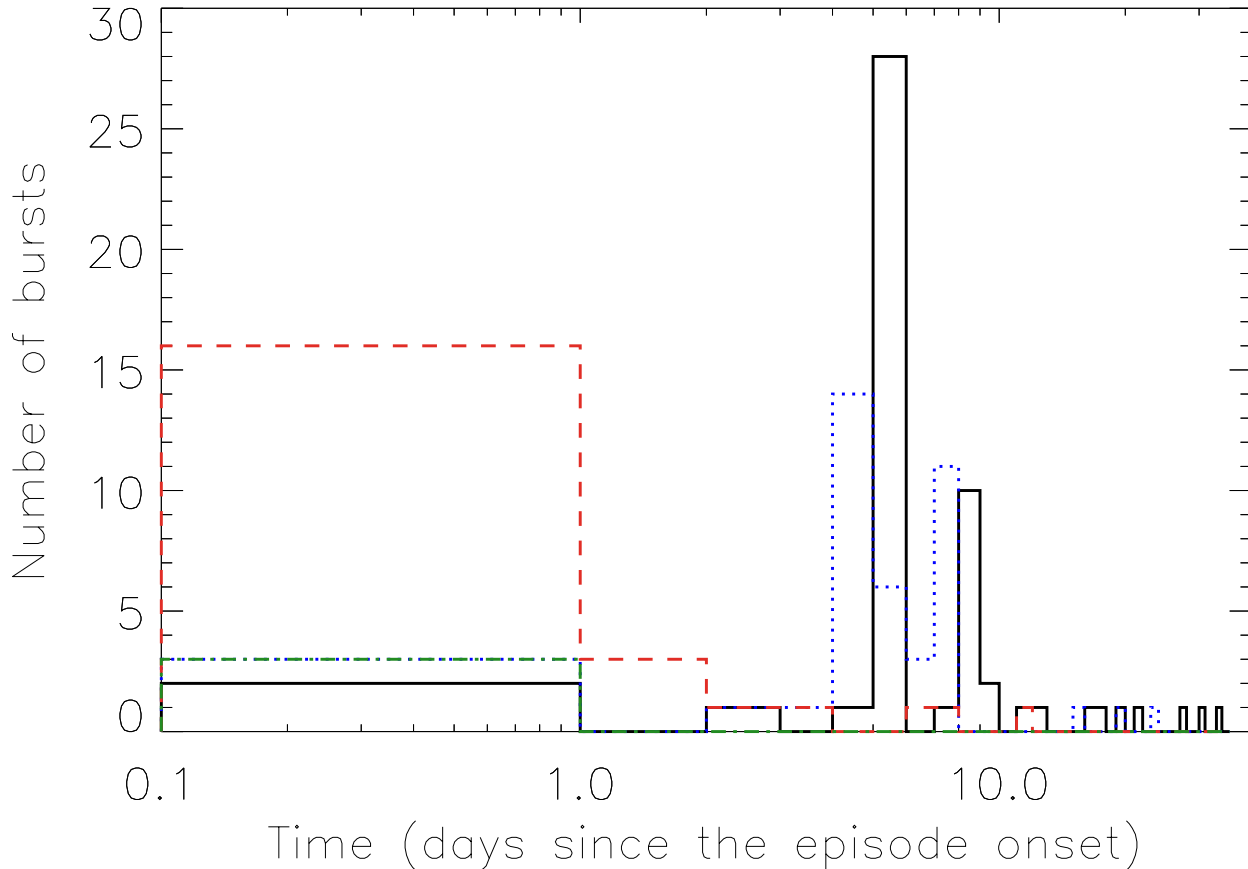


**Figure 9.** The number of bursts in each active episode of SGR J1935+2154. The blue dashed-dotted line, red dashed line, blue dotted line and the black solid line represent the first, second, third and fourth active burst episodes, respectively.

**Table 6.** Mean parameters of GBM bursts during all active episodes.

Episode	$\langle T_{\text{bb}} \rangle$ (ms)	$\langle \text{Fluence} \rangle$ ( $10^{-7} \text{erg cm}^{-2}$ )	BB+BB		COMPT	
			$\langle \text{low } kT \rangle$ (keV)	$\langle \text{high } kT \rangle$ (keV)	$\langle E_{\text{peak}} \rangle$ (keV)	$\langle \text{index} \rangle$
2	$78^{+17}_{-14}$	$1.1^{+0.4}_{-0.3}$	$4.1 \pm 0.1$	$11.2 \pm 0.3$	$30.0 \pm 0.4$	$0.18 \pm 0.10$
3	$72^{+7}_{-6}$	$0.7 \pm 0.2$	$5.4 \pm 0.2$	$13.3 \pm 0.9$	$33.8 \pm 1.3$	$0.07 \pm 0.05$
4	$128^{+11}_{-10}$	$0.9^{+0.3}_{-0.2}$	$5.1 \pm 0.1$	$12.1 \pm 0.4$	$30.4 \pm 0.2$	$-0.02 \pm 0.26$

We also studied the distributions of temporal and spectral parameters of the bursts from each of the four active episodes (Figure 10). The mean values of the Gaussian or log-Gaussian fits to these distributions during the 2<sup>nd</sup>, 3<sup>rd</sup> and 4<sup>th</sup> episodes, are listed in Table 6. The duration of bursts from the 2<sup>nd</sup> and 3<sup>rd</sup> episodes are shorter than the 4<sup>th</sup>, while the average fluences are consistent (within error). Both BB temperatures from the BB+BB model are lower before 2016. Similar time evolution of burst characteristics was also reported for SGR J1550–5418 (von Kienlin et al. 2012).

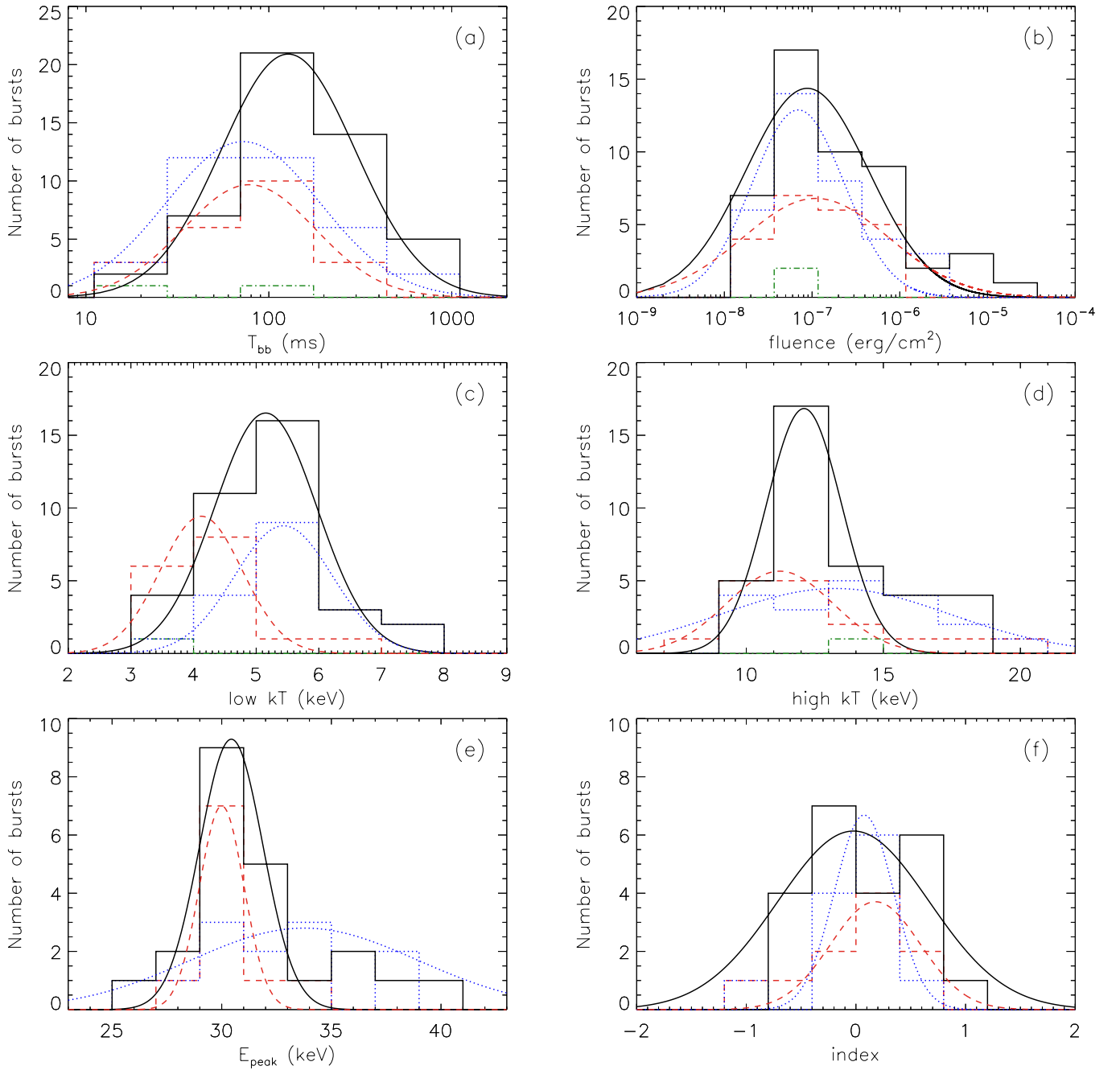


**Figure 10.** Distributions of  $T_{bb}$  (a), fluence (b), along with the low (c) and high (d) temperature from fits using a BB+BB model fit are presented in the top and middle two panels, respectively. The  $E_{\text{peak}}$  (e) and index (f) distributions from fits to SGR J1935+2154 bursts using the COMPT model observed by GBM, are presented in the bottom two panels. The green dashed-dotted, red dashed, blue dotted and black solid histograms represent burst active episodes 1 through 4, respectively. The best Gaussian or log-Gaussian fits to the histograms are over-plotted in each panel.

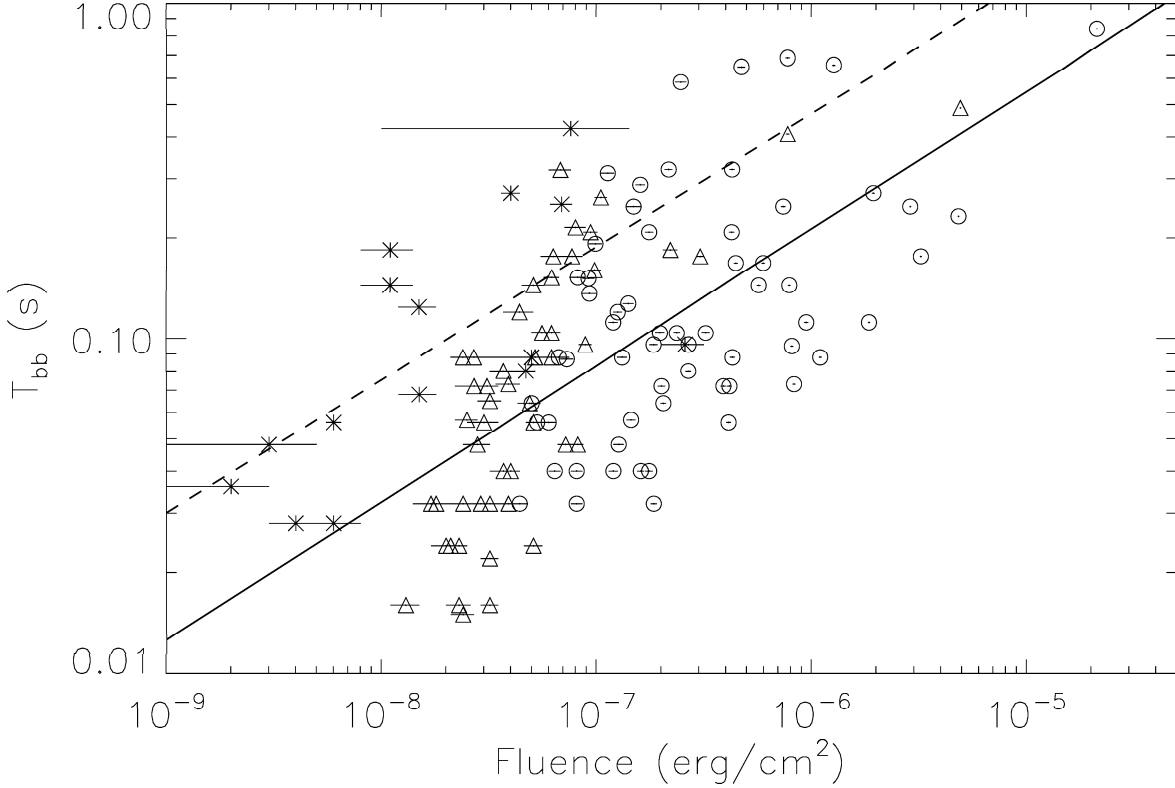


**Figure 11.** The correlation between  $T_{bb}$  and energy fluence. The stars, open circles and triangles represent BAT bursts, GBM triggered bursts and GBM un-triggered bursts, respectively. The dashed line is the best PL fit to 15 bursts only observed with the BAT. The solid line is the same fit to 112 GBM events.

#### 4.4. Burst properties and correlations

In previous studies, the short burst duration distributions ( $T_{90}$ ) followed a log-Gaussian shape, reaching a peak at  $\sim 90 - 160$  ms (Gögüş et al. 2001; Gavriil et al. 2004; Lin et al. 2011a; van der Horst et al. 2012; Collazzi et al. 2015). The  $T_{bb}$  of bursts from SGR J1935+2154 also followed a log-Gaussian distribution, with a mean value of  $\sim 94$  ms. Although,  $T_{bb}$  is typically longer than  $T_{90}$ , we find  $\langle T_{bb} \rangle$  for our sample to be at the lower end of known values. The mean  $T_{90}$  from a log-Gaussian fit results in  $\sim 75$  ms, which is about two-thirds of the typical value for other magnetars.

The correlation between the burst duration and fluence has been previously reported for several magnetars (Gögüş et al. 2001; Gavriil et al. 2004; van der Horst et al. 2012). For bursts from SGR J1935+2154, we also find that  $T_{bb}$  is significantly correlated with energy fluence (Figure 11). The Spearman rank correlation test coefficient is 0.6, with a chance probability of  $1.2 \times 10^{-14}$  for 112 GBM bursts. We fit this correlation with a PL and find the index to be  $0.41 \pm 0.04$  (using GBM bursts) and  $0.40 \pm 0.13$  (using only BAT detected bursts), in very good agreement with each other. These values are also consistent with similar values for SGR 1806–20, SGR 1900+14 (Gögüş et al. 2001) and SGR J1550–5418 (van der Horst et al. 2012), while being shallower than 1E 2259+586 (Gavriil et al. 2004).

There are 80 bursts in our sample whose data is well fit using a BB+BB model. The temperatures of the two blackbody components are consistent with those reported for other magnetars (e.g., Lin



et al. 2011a; van der Horst et al. 2012; Collazzi et al. 2015). We do not find a correlation between the temperatures of the two BB components. Kozlova et al. (2016) fit the time-integrated spectrum between 20 – 300 keV for the intermediate flare from SGR J1935+2154 with the same model. They found a similar temperature for the hard BB component, and a higher temperature ( $\sim 6.4$  keV) for the soft BB component. The difference may be due to the low-energy cutoff of the spectrum, which is 10 keV more than that of GBM.

The relationship between the BB emission areas ( $R^2$ ), and temperatures (see the lower right panel of Figure 6), indicates that the hotter BB components are from a smaller area. The Spearman test yields a correlation coefficient of -0.8 with a chance probability of  $1.1 \times 10^{-20}$ . We fit this correlation with a PL and obtain an index of  $-10.6 \pm 1.8$ . The correlation for the cooler BB components is not significant. The emission area of the cool component spreads around a mean value of  $\sim 161$  km<sup>2</sup>. If we describe both BB components with one PL, the index for the best fit is  $-4.2 \pm 0.3$ , which is consistent with the index of a BB with steady luminosity. These results agree with those for other magnetars, e.g., SGR J1550–5418 (van der Horst et al. 2012) and SGR J0501+4516 (Lin et al. 2011a). The evolution of the emission area with BB temperature, the strong correlation between the emission areas and luminosities of both BB components (Figure 6), as well as the equally divided energy for both BB fits, possibly indicates that the two BB components are strongly connected events despite emanating from very different regions. As discussed in van der Horst et al. (2012); Younes et al. (2014), a detailed modeling of the dynamic fireball in the magnetosphere is required to understand the actual physical process.

The  $E_{peak}$  and PL index of the COMPT model are quite different for SGR J1935+2154 when compared with other magnetars. The distribution of  $E_{peak}$  values for all bursts peaks at  $\sim 30$  keV, which is softer than SGR J1550–5418 (van der Horst et al. 2012) and SGR J0501+4516 (Lin et al. 2011a) ( $\sim 40$  keV). In the Comptonization process, the photons can be scattered up to a higher energy consistent with the electron temperature. The softer  $E_{peak}$  indicates that either the temperature of the plasma covering SGR J1935+2154 is slightly cooler than other magnetars or, the SGR J1935+2154 bursts are emitted from a relatively cooler region of SGR J1935+2154.

The average spectral index is  $\sim -0.1$ , similar to that of bursts from SGR J0501+4516 (Lin et al. 2011a), while harder than the index measured in SGR J1550–5418 bursts ( $\sim -1$ ) (van der Horst et al. 2012). As discussed in Lin et al. (2011a), the index of Compton up-scattering depends on the mean energy change per collision and the mean amount of scattering. However, this parameter can change in magnetars due to the presence of a strong magnetic field. The evolution of index with burst fluence is also very interesting. The dimmer bursts present the flattest spectrum that can be produced with Compton up-scattering, while the brighter bursts exhibit a more thermalized environment. A similar correlation was only reported by Younes et al. (2014), who studied the time-resolved spectra of SGR J1550 – 5418. These results stress that time-resolved analysis is crucial in understanding how the emission properties evolve through a magnetar burst. We will present the results of the time-resolved analysis for SGR J1935+2154 bursts in an upcoming paper.

**Table 4.** The Duration, Localization and Fluence for each SGR J1935+2154 burst.

ID	Instrument	$t_{burst}$ in UTC	$T_{BB}$ (s)	$T_{90}$ (s)	$T_{50}$ (s)	ra ( $^{\circ}$ )	dec ( $^{\circ}$ )	err ( $^{\circ}$ )	Fluence ( $10^{-7}$ erg $\text{cm}^{-2}$ )
1	GBM <sup>U</sup> BAT <sup>T</sup>	2014-07-05 09:32:48.643	0.088	0.112 $\pm$ 0.051	0.048 $\pm$ 0.011	297.28	18.18	6.57	0.62 $\pm$ 0.05
2	GBM <sup>U</sup> BAT <sup>U</sup>	2014-07-05 09:37:34.484	0.022	0.024 $\pm$ 0.040	0.008 $\pm$ 0.011	291.63	20.72	9.65	0.32 $\pm$ 0.03
3	BAT <sup>U</sup>	2014-07-05 09:41:06.139	0.124	...	...	...	...	...	0.41 $\pm$ 0.26
4	BAT <sup>T</sup>	2015-02-22 12:16:26.304	0.088	...	...	...	...	...	0.30 $\pm$ 0.03
5	BAT <sup>T</sup>	2015-02-22 12:31:11.348	0.080	...	...	...	...	...	0.15 $\pm$ 0.03
6	GBM <sup>U</sup>	2015-02-22 07:16:56.058	0.016	0.008 $\pm$ 0.029	0.000 $\pm$ 0.011	305.65	15.84	11.93	0.13 $\pm$ 0.02
7	GBM <sup>U</sup>	2015-02-22 08:40:13.706	0.048	0.032 $\pm$ 0.018	0.016 $\pm$ 0.023	296.05	18.81	4.19	0.82 $\pm$ 0.05
8	GBM <sup>U</sup>	2015-02-22 13:33:00.033	0.048	FAIL	FAIL	300.82	32.16	3.95	0.28 $\pm$ 0.04
9	GBM <sup>U</sup>	2015-02-22 14:33:20.243	0.264	0.248 $\pm$ 0.023	0.152 $\pm$ 0.018	295.53	17.69	4.96	1.05 $\pm$ 0.07
10	GBM <sup>T</sup>	2015-02-22 17:57:05.950	0.096	0.064 $\pm$ 0.011	0.024 $\pm$ 0.011	304.59	19.51	3.70	1.85 $\pm$ 0.08
11	GBM <sup>U</sup>	2015-02-22 19:24:45.954	0.024	0.064 $\pm$ 0.029	0.016 $\pm$ 0.011	296.96	8.68	11.34	0.20 $\pm$ 0.03
12	GBM <sup>T</sup>	2015-02-22 19:44:16.881	0.040	0.040 $\pm$ 0.011	0.016 $\pm$ 0.011	295.57	21.97	1.45	1.76 $\pm$ 0.07
13	GBM <sup>U</sup>	2015-02-22 19:58:16.658	0.104	0.104 $\pm$ 0.025	0.040 $\pm$ 0.029	302.90	29.42	4.33	0.62 $\pm$ 0.06
14	GBM <sup>U</sup>	2015-02-22 20:47:02.245	0.024	0.032 $\pm$ 0.047	0.008 $\pm$ 0.011	302.02	18.95	10.38	0.21 $\pm$ 0.03
15	GBM <sup>U</sup>	2015-02-22 23:57:33.875	0.152	0.136 $\pm$ 0.018	0.064 $\pm$ 0.011	288.57	22.29	5.52	0.62 $\pm$ 0.05
16	GBM <sup>T</sup>	2015-02-23 01:38:07.938	0.112	0.072 $\pm$ 0.011	0.040 $\pm$ 0.011	293.00	18.76	1.67	9.48 $\pm$ 0.22
17	GBM <sup>U</sup>	2015-02-23 05:05:06.514	0.032	0.032 $\pm$ 0.036	0.008 $\pm$ 0.011	292.45	31.86	7.12	0.32 $\pm$ 0.03
18	GBM <sup>T</sup>	2015-02-23 05:24:53.876	0.320	0.288 $\pm$ 0.153	0.128 $\pm$ 0.018	293.24	21.93	1.80	2.17 $\pm$ 0.09
19	GBM <sup>T</sup>	2015-02-23 06:45:40.113	0.088	0.080 $\pm$ 0.041	0.024 $\pm$ 0.011	299.60	18.06	1.71	4.30 $\pm$ 0.11
20	GBM <sup>U</sup>	2015-02-23 14:26:16.236	0.048	0.096 $\pm$ 0.025	0.024 $\pm$ 0.011	295.65	16.37	7.55	0.72 $\pm$ 0.06

Table 4 continued on next page

Table 4 (continued)

ID	Instrument	$t_{burst}$ in UTC	$T_{BB}$ (s)	$T_{90}$ (s)	$T_{50}$ (s)	ra ( $^{\circ}$ )	dec ( $^{\circ}$ )	err ( $^{\circ}$ )	Fluence ( $10^{-7}$ erg $\text{cm}^{-2}$ )
21	GBM <sup>T</sup>	2015-02-23 16:13:52.464	0.088	0.088 ± 0.064	0.016 ± 0.011	291.40	18.64	4.62	1.32 ± 0.07
22	GBM <sup>T</sup>	2015-02-24 06:48:47.147	0.064	0.080 ± 0.036	0.040 ± 0.018	291.43	15.63	7.09	0.50 ± 0.04
23	GBM <sup>T</sup>	2015-02-24 22:46:34.025	0.032	0.112 ± 0.018	0.024 ± 0.011	293.82	27.13	2.90	0.44 ± 0.04
24	GBM <sup>T</sup>	2015-02-25 10:51:03.576	0.104	0.096 ± 0.023	0.032 ± 0.011	296.09	11.67	3.38	3.23 ± 0.14
25	GBM <sup>T</sup>	2015-02-28 10:56:48.801	0.208	0.040 ± 0.011	0.024 ± 0.018	297.22	20.83	1.00	4.26 ± 0.12
26	GBM <sup>T</sup>	2015-03-01 07:28:54.127	0.072	0.040 ± 0.018	0.024 ± 0.011	293.23	18.79	1.35	4.16 ± 0.10
27	GBM <sup>T</sup>	2015-03-05 18:59:19.838	0.072	0.056 ± 0.011	0.024 ± 0.011	295.08	19.65	3.08	2.01 ± 0.08
28	GBM <sup>T</sup>	2016-02-01 09:37:15.695	0.040	0.032 ± 0.041	0.016 ± 0.011	291.10	17.80	4.59	1.20 ± 0.06
29	GBM <sup>T</sup>	2016-05-14 08:21:54.660	0.087	0.080 ± 0.031	0.028 ± 0.025	302.17	27.25	5.65	0.73 ± 0.05
30	GBM <sup>U</sup>	2016-05-14 16:13:47.362	0.057	0.104 ± 0.034	0.032 ± 0.018	298.64	20.15	7.26	0.25 ± 0.03
31	GBM <sup>U</sup>	2016-05-14 22:25:21.843	0.015	FAIL	FAIL	279.91	19.23	11.49	0.24 ± 0.03
32	GBM <sup>T</sup>	2016-05-16 20:49:46.978	0.032	0.036 ± 0.029	0.012 ± 0.011	295.24	25.13	2.99	0.81 ± 0.05
	BAT <sup>T</sup>		0.028	...	...	...	...	...	0.39 ± 0.10
33	GBM <sup>U</sup>	2016-05-18 07:49:33.972	0.176	0.168 ± 0.069	0.104 ± 0.040	296.54	19.89	10.99	0.63 ± 0.08
34	GBM <sup>T</sup>	2016-05-18 08:37:07.516	0.152	0.144 ± 0.011	0.088 ± 0.023	287.37	16.54	5.45	0.82 ± 0.07
35	BAT <sup>U</sup>	2016-05-18 09:06:21.839	0.144	...	...	...	...	...	0.11 ± 0.03
36	GBM <sup>T</sup>	2016-05-18 09:09:23.800	0.248	0.128 ± 0.011	0.064 ± 0.011	295.28	18.46	1.00	28.84 ± 0.22
	BAT <sup>T</sup>		0.168	...	...	...	...	...	17.00 ± 2.69
37	GBM <sup>T</sup>	2016-05-18 10:07:26.744	0.056	0.096 ± 0.023	0.032 ± 0.011	297.32	28.96	7.46	0.53 ± 0.06
38	GBM <sup>T</sup>	2016-05-18 10:28:02.817	0.104	0.088 ± 0.018	0.024 ± 0.011	294.02	21.68	2.02	2.37 ± 0.08
39	GBM <sup>T</sup>	2016-05-18 14:59:31.080	0.072	0.048 ± 0.025	0.024 ± 0.011	293.67	26.30	2.11	3.90 ± 0.12
40	GBM <sup>T</sup>	2016-05-18 15:33:47.010	0.056	0.064 ± 0.025	0.024 ± 0.011	293.02	21.90	4.66	0.60 ± 0.05
41	GBM <sup>T</sup>	2016-05-18 17:00:31.760	0.120	0.120 ± 0.036	0.024 ± 0.023	297.73	26.52	4.41	1.26 ± 0.06
42	GBM <sup>U</sup>	2016-05-18 17:05:12.813	0.088	0.064 ± 0.029	0.040 ± 0.023	295.26	15.45	12.68	0.24 ± 0.03

Table 4 continued on next page

Table 4 (continued)

ID	Instrument	$t_{burst}$ in UTC	$T_{BB}$ (s)	$T_{90}$ (s)	$T_{50}$ (s)	ra ( $^{\circ}$ )	dec ( $^{\circ}$ )	err ( $^{\circ}$ )	Fluence ( $10^{-7}$ erg $\text{cm}^{-2}$ )
43	GBM <sup>U</sup>	2016-05-18 18:33:55.525	0.016	0.032 $\pm$ 0.033	0.016 $\pm$ 0.023	298.64	19.89	3.76	0.32 $\pm$ 0.03
44	GBM <sup>T</sup>	2016-05-18 19:40:37.470	0.584	0.496 $\pm$ 0.116	0.152 $\pm$ 0.029	289.14	20.30	2.92	2.47 $\pm$ 0.15
45	GBM <sup>U</sup>	2016-05-18 22:07:13.367	0.064	0.064 $\pm$ 0.025	0.040 $\pm$ 0.011	270.10	33.13	10.59	0.49 $\pm$ 0.06
46	GBM <sup>T</sup>	2016-05-19 00:34:15.887	0.040	0.032 $\pm$ 0.045	0.016 $\pm$ 0.025	293.31	28.89	3.56	0.64 $\pm$ 0.04
47	GBM <sup>U</sup>	2016-05-19 05:41:25.858	0.065	0.064 $\pm$ 0.018	0.016 $\pm$ 0.011	296.36	20.70	6.78	0.32 $\pm$ 0.04
	BAT <sup>T</sup>		0.016	...	...	...	...	...	0.08 $\pm$ 0.02
48	GBM <sup>U</sup>	2016-05-19 11:46:52.546	0.024	0.024 $\pm$ 0.041	0.008 $\pm$ 0.023	290.55	14.69	5.42	0.23 $\pm$ 0.02
49	GBM <sup>U</sup>	2016-05-19 11:59:32.632	0.056	0.056 $\pm$ 0.029	0.024 $\pm$ 0.018	288.74	28.32	5.96	0.51 $\pm$ 0.04
50	GBM <sup>T</sup>	2016-05-19 12:07:46.594	0.064	0.064 $\pm$ 0.029	0.016 $\pm$ 0.018	289.65	19.47	2.30	2.05 $\pm$ 0.06
51	GBM <sup>U</sup>	2016-05-19 19:59:54.938	0.319	0.328 $\pm$ 0.025	0.304 $\pm$ 0.011	290.10	18.45	7.48	0.68 $\pm$ 0.08
52	GBM <sup>U</sup>	2016-05-20 03:24:12.830	0.040	0.040 $\pm$ 0.011	0.024 $\pm$ 0.011	291.51	19.16	9.67	0.37 $\pm$ 0.05
53	GBM <sup>T</sup>	2016-05-20 05:21:33.483	0.112	0.088 $\pm$ 0.011	0.048 $\pm$ 0.011	287.44	19.53	1.38	18.56 $\pm$ 0.19
54	GBM <sup>T</sup>	2016-05-20 16:21:43.172	0.095	0.080 $\pm$ 0.058	0.024 $\pm$ 0.011	297.64	14.80	1.87	8.13 $\pm$ 0.13
55	GBM <sup>T</sup>	2016-05-20 21:42:29.323	0.272	0.200 $\pm$ 0.018	0.040 $\pm$ 0.011	287.99	15.84	1.50	19.44 $\pm$ 0.30
56	GBM <sup>T</sup>	2016-05-21 03:23:36.644	0.040	0.024 $\pm$ 0.025	0.008 $\pm$ 0.018	294.66	28.06	1.90	1.61 $\pm$ 0.06
57	GBM <sup>T</sup>	2016-05-21 11:42:41.548	0.248	0.200 $\pm$ 0.011	0.072 $\pm$ 0.011	292.99	25.55	1.46	7.40 $\pm$ 0.16
58	BAT <sup>T</sup>	2016-05-21 20:01:47.342	0.068	...	...	...	...	...	0.15 $\pm$ 0.03
59	BAT <sup>U</sup>	2016-05-21 20:10:34.402	0.048	...	...	...	...	...	0.03 $\pm$ 0.02
60	BAT <sup>U</sup>	2016-05-21 20:17:15.638	0.184	...	...	...	...	...	0.11 $\pm$ 0.03
61	BAT <sup>U</sup>	2016-05-21 20:21:03.566	0.028	...	...	...	...	...	0.04 $\pm$ 0.01
62	BAT <sup>U</sup>	2016-05-21 20:22:27.066	0.036	...	...	...	...	...	0.02 $\pm$ 0.01
63	BAT <sup>T</sup>	2016-05-21 20:23:42.298	0.252	...	...	...	...	...	0.69 $\pm$ 0.08
64	GBM <sup>T</sup>	2016-05-21 20:43:09.516	0.688	0.648 $\pm$ 0.011	0.056 $\pm$ 0.018	291.30	18.37	1.21	7.76 $\pm$ 0.19
65	GBM <sup>T</sup>	2016-05-21 21:13:16.242	0.040	0.040 $\pm$ 0.047	0.008 $\pm$ 0.011	290.53	21.33	1.75	0.81 $\pm$ 0.05

Table 4 continued on next page

Table 4 (continued)

ID	Instrument	$t_{burst}$ in UTC	$T_{BB}$ (s)	$T_{90}$ (s)	$T_{50}$ (s)	ra ( $^{\circ}$ )	dec ( $^{\circ}$ )	err ( $^{\circ}$ )	Fluence ( $10^{-7}$ erg $\text{cm}^{-2}$ )
66	GBM <sup>T</sup>	2016-05-22 00:12:59.206	0.032	0.088 ± 0.096	0.008 ± 0.011	294.10	20.09	1.54	1.85 ± 0.06
67	GBM <sup>U</sup>	2016-05-22 03:11:17.452	0.032	0.072 ± 0.047	0.024 ± 0.011	274.87	5.39	13.02	0.18 ± 0.03
68	GBM <sup>U</sup>	2016-05-30 00:46:25.803	0.184	0.184 ± 0.029	0.144 ± 0.018	294.69	19.85	4.26	2.21 ± 0.17
69	GBM <sup>T</sup>	2016-06-02 12:19:30.674	0.127	0.088 ± 0.011	0.024 ± 0.023	295.34	18.40	3.90	1.41 ± 0.08
70	GBM <sup>U</sup>	2016-06-06 21:41:54.098	0.032	0.032 ± 0.040	0.016 ± 0.018	294.91	27.52	7.94	0.29 ± 0.03
71	GBM <sup>U</sup>	2016-06-18 01:42:55.569	0.024	0.048 ± 0.018	0.016 ± 0.018	303.27	24.87	10.99	0.51 ± 0.05
72	GBM <sup>T</sup>	2016-06-18 20:27:25.778	0.088	0.064 ± 0.011	0.032 ± 0.011	293.76	20.69	1.47	11.01 ± 0.15
73	GBM <sup>T</sup>	2016-06-20 15:16:34.838	0.232	0.176 ± 0.011	0.096 ± 0.011	292.82	20.37	1.00	48.36 ± 0.32
74	GBM <sup>T</sup>	2016-06-22 13:45:23.754	0.112	0.104 ± 0.041	0.040 ± 0.018	294.69	18.44	3.83	1.20 ± 0.06
75	BAT <sup>U</sup>	2016-06-23 19:22:15.489	0.056	...	...	...	...	...	0.06 ± 0.00
76	BAT <sup>T</sup>	2016-06-23 19:24:40.061	0.096	...	...	...	...	...	2.59 ± 0.58
77	BAT <sup>U</sup>	2016-06-23 19:36:27.365	0.272	...	...	...	...	...	0.40 ± 0.04
78	BAT <sup>U</sup>	2016-06-23 19:37:59.837	0.424	...	...	...	...	...	0.76 ± 0.66
79	GBM <sup>T</sup>	2016-06-23 15:16:09.020	0.248	0.192 ± 0.082	0.056 ± 0.023	300.52	14.65	5.84	1.49 ± 0.11
80	GBM <sup>U</sup>	2016-06-23 15:16:26.836	0.176	0.168 ± 0.018	0.088 ± 0.011	298.81	18.77	3.39	3.04 ± 0.11
81	GBM <sup>U</sup>	2016-06-23 16:17:04.220	0.073	0.072 ± 0.038	0.032 ± 0.018	287.62	15.04	8.99	0.39 ± 0.05
82	GBM <sup>T</sup>	2016-06-23 16:49:57.493	0.168	0.096 ± 0.025	0.048 ± 0.011	291.66	22.66	1.68	4.45 ± 0.10
83	GBM <sup>T</sup>	2016-06-23 17:39:22.327	0.104	0.072 ± 0.018	0.032 ± 0.018	295.55	29.03	6.85	1.98 ± 0.10
84	GBM <sup>U</sup>	2016-06-23 17:47:06.896	0.032	0.040 ± 0.047	0.008 ± 0.011	304.32	34.07	9.16	0.24 ± 0.04
85	GBM <sup>U</sup>	2016-06-23 17:55:48.768	0.080	0.080 ± 0.011	0.056 ± 0.025	289.63	24.21	7.92	0.37 ± 0.05
86	GBM <sup>U</sup>	2016-06-23 17:58:55.696	0.072	0.088 ± 0.040	0.048 ± 0.018	300.15	18.28	12.06	0.31 ± 0.04
87	GBM <sup>U</sup>	2016-06-23 18:22:43.425	0.104	0.136 ± 0.069	0.072 ± 0.018	308.86	14.91	8.30	0.56 ± 0.06
88	GBM <sup>T</sup>	2016-06-23 19:24:40.061	0.056	0.040 ± 0.011	0.024 ± 0.011	293.47	17.65	1.61	4.12 ± 0.10
89	GBM <sup>U</sup>	2016-06-23 19:36:27.341	0.176	0.224 ± 0.057	0.120 ± 0.023	283.79	11.95	9.89	0.77 ± 0.09

Table 4 continued on next page

Table 4 (continued)

ID	Instrument	$t_{burst}$ in UTC	$T_{BB}$ (s)	$T_{90}$ (s)	$T_{50}$ (s)	ra ( $^{\circ}$ )	dec ( $^{\circ}$ )	err ( $^{\circ}$ )	Fluence ( $10^{-7}$ erg $\text{cm}^{-2}$ )
90	GBM <sup>T</sup>	2016-06-23 19:37:59.997	0.136	0.184 $\pm$ 0.018	0.112 $\pm$ 0.018	289.98	26.72	6.30	0.93 $\pm$ 0.08
91	GBM <sup>U</sup>	2016-06-23 19:51:16.261	0.120	0.104 $\pm$ 0.036	0.064 $\pm$ 0.018	292.19	26.72	10.71	0.44 $\pm$ 0.07
92	GBM <sup>T</sup>	2016-06-23 20:06:37.158	0.096	0.072 $\pm$ 0.018	0.024 $\pm$ 0.011	294.46	27.37	1.40	2.69 $\pm$ 0.09
93	GBM <sup>T</sup>	2016-06-23 21:12:29.780	0.168	0.104 $\pm$ 0.023	0.032 $\pm$ 0.011	293.10	17.42	2.25	5.97 $\pm$ 0.11
94	GBM <sup>U</sup>	2016-06-23 21:15:31.444	0.160	0.160 $\pm$ 0.028	0.032 $\pm$ 0.018	291.75	17.13	6.35	0.98 $\pm$ 0.07
95	GBM <sup>U</sup>	2016-06-23 21:16:24.612	0.408	0.344 $\pm$ 0.018	0.032 $\pm$ 0.011	293.04	17.87	1.66	7.77 $\pm$ 0.14
96	GBM <sup>U</sup>	2016-06-23 21:20:46.404	0.488	0.418 $\pm$ 0.011	0.256 $\pm$ 0.011	290.46	17.32	1.52	49.38 $\pm$ 0.28
97	GBM <sup>T</sup>	2016-06-23 21:23:36.780	0.144	0.104 $\pm$ 0.011	0.048 $\pm$ 0.011	293.58	19.84	1.00	7.90 $\pm$ 0.11
98	GBM <sup>U</sup>	2016-06-23 21:30:47.032	0.208	0.320 $\pm$ 0.058	0.112 $\pm$ 0.018	292.56	12.86	6.75	0.94 $\pm$ 0.07
99	GBM <sup>U</sup>	2016-06-23 21:31:12.600	0.096	0.104 $\pm$ 0.018	0.064 $\pm$ 0.025	299.07	14.21	6.00	0.89 $\pm$ 0.06
100	GBM <sup>U</sup>	2016-06-23 21:38:13.432	0.056	0.056 $\pm$ 0.062	0.048 $\pm$ 0.018	310.34	13.04	12.79	0.30 $\pm$ 0.05
101	GBM <sup>T</sup>	2016-06-23 22:41:58.592	0.144	0.088 $\pm$ 0.018	0.024 $\pm$ 0.011	288.49	20.48	1.37	5.69 $\pm$ 0.12
102	GBM <sup>U</sup>	2016-06-24 00:49:23.678	0.072	0.064 $\pm$ 0.158	0.032 $\pm$ 0.158	310.04	17.71	14.51	0.27 $\pm$ 0.05
103	GBM <sup>T</sup>	2016-06-25 08:04:52.961	0.320	0.072 $\pm$ 0.018	0.024 $\pm$ 0.011	293.17	17.65	1.62	4.28 $\pm$ 0.12
104	GBM <sup>T</sup>	2016-06-26 05:15:20.628	0.192	0.184 $\pm$ 0.033	0.040 $\pm$ 0.033	289.91	21.08	3.05	0.99 $\pm$ 0.07
105	GBM <sup>T</sup>	2016-06-26 06:03:14.969	0.208	0.192 $\pm$ 0.029	0.104 $\pm$ 0.058	294.23	20.76	1.14	1.76 $\pm$ 0.08
106	GBM <sup>T</sup>	2016-06-26 09:40:11.887	0.656	0.160 $\pm$ 0.018	0.040 $\pm$ 0.011	289.90	21.02	1.22	12.72 $\pm$ 0.19
107	GBM <sup>U</sup>	2016-06-26 11:22:27.435	0.215	0.216 $\pm$ 0.075	0.120 $\pm$ 0.058	296.00	22.41	4.04	0.80 $\pm$ 0.09
108	GBM <sup>T</sup>	2016-06-26 13:54:30.722	0.840	0.688 $\pm$ 0.011	0.376 $\pm$ 0.011	296.46	20.05	1.00	213.12 $\pm$ 0.74
	BAT <sup>T</sup>		0.892	...	...	...	...	...	116.99 $\pm$ 4.42
109	BAT <sup>T</sup>	2016-06-26 14:04:02.655	0.028	...	...	...	...	...	0.06 $\pm$ 0.02
110	GBM <sup>T</sup>	2016-06-26 17:22:55.139	0.088	0.088 $\pm$ 0.041	0.040 $\pm$ 0.018	290.09	21.75	2.64	0.67 $\pm$ 0.06
111	GBM <sup>U</sup>	2016-06-26 17:50:03.251	0.032	0.048 $\pm$ 0.029	0.024 $\pm$ 0.018	294.83	22.39	1.76	0.39 $\pm$ 0.04
112	GBM <sup>U</sup>	2016-06-26 18:57:10.380	0.016	0.056 $\pm$ 0.089	0.016 $\pm$ 0.011	298.58	15.73	7.66	0.23 $\pm$ 0.03

Table 4 continued on next page

Table 4 (continued)

ID	Instrument	$t_{burst}$ in UTC	$T_{BB}$ (s)	$T_{90}$ (s)	$T_{50}$ (s)	ra ( $^{\circ}$ )	dec ( $^{\circ}$ )	err ( $^{\circ}$ )	Fluence ( $10^{-7}$ erg $\text{cm}^{-2}$ )
113	GBM <sup>U</sup>	2016-06-26 20:34:49.312	0.040	0.080 $\pm$ 0.049	0.040 $\pm$ 0.011	294.82	22.37	2.50	0.40 $\pm$ 0.04
114	GBM <sup>T</sup>	2016-06-27 01:50:15.847	0.080	0.080 $\pm$ 0.018	0.032 $\pm$ 0.011	290.89	20.60	1.05	2.68 $\pm$ 0.08
115	GBM <sup>U</sup>	2016-06-27 09:44:07.706	0.088	0.080 $\pm$ 0.018	0.024 $\pm$ 0.011	294.21	20.71	5.14	0.52 $\pm$ 0.05
116	GBM <sup>U</sup>	2016-06-29 18:32:06.379	0.032	0.040 $\pm$ 0.034	0.024 $\pm$ 0.023	289.90	23.42	8.65	0.17 $\pm$ 0.03
117	GBM <sup>T</sup>	2016-06-30 10:02:25.999	0.057	0.056 $\pm$ 0.018	0.032 $\pm$ 0.011	292.88	17.30	2.09	1.45 $\pm$ 0.07
118	GBM <sup>T</sup>	2016-07-04 14:33:38.653	0.073	0.048 $\pm$ 0.011	0.032 $\pm$ 0.011	295.60	21.98	1.36	8.31 $\pm$ 0.12
119	GBM <sup>U</sup>	2016-07-05 13:50:34.167	0.144	0.112 $\pm$ 0.080	0.080 $\pm$ 0.033	295.20	22.09	13.13	0.51 $\pm$ 0.06
120	GBM <sup>U</sup>	2016-07-07 07:40:59.986	0.088	0.080 $\pm$ 0.036	0.048 $\pm$ 0.018	290.27	19.61	12.85	0.27 $\pm$ 0.04
121	GBM <sup>T</sup>	2016-07-09 16:54:28.219	0.312	0.288 $\pm$ 0.018	0.272 $\pm$ 0.018	291.64	20.05	5.03	1.13 $\pm$ 0.08
122	GBM <sup>T</sup>	2016-07-15 07:09:11.722	0.072	0.072 $\pm$ 0.023	0.032 $\pm$ 0.011	295.23	23.29	2.58	2.01 $\pm$ 0.07
123	GBM <sup>T</sup>	2016-07-18 09:36:06.543	0.648	0.616 $\pm$ 0.011	0.576 $\pm$ 0.011	287.26	18.90	3.34	4.73 $\pm$ 0.19
124	GBM <sup>T</sup>	2016-07-21 09:36:13.665	0.176	0.152 $\pm$ 0.011	0.096 $\pm$ 0.011	292.46	21.25	1.00	32.32 $\pm$ 0.26
125	GBM <sup>T</sup>	2016-08-05 04:51:17.143	0.048	0.032 $\pm$ 0.038	0.024 $\pm$ 0.018	288.05	19.10	6.73	1.27 $\pm$ 0.07
126	GBM <sup>T</sup>	2016-08-25 07:26:53.513	0.288	0.184 $\pm$ 0.018	0.144 $\pm$ 0.018	296.35	25.07	2.74	1.60 $\pm$ 0.08
127	GBM <sup>T</sup>	2016-08-26 14:05:52.955	0.151	0.120 $\pm$ 0.049	0.096 $\pm$ 0.025	293.94	26.11	3.98	0.92 $\pm$ 0.06

**Table 5.** Spectral fit parameters for all SGR J1935+2154 bursts.

ID	Instrument	BB+BB or BB		COMPT or PL			OTTB		
		k $\Gamma_1$ (keV)	k $\Gamma_2$ (keV)	$\chi^2/d.o.f$	$\Gamma$	k $\Gamma$ (keV)	$\chi^2/d.o.f$	k $\Gamma$ (keV)	$\chi^2/d.o.f$
1	GBM <sup>U</sup>	3.31 <sup>+0.58</sup> <sub>-0.60</sub>	13.38 <sup>+2.01</sup> <sub>-1.80</sub>	316.69/265	-2.35 <sup>+0.10</sup> <sub>-0.11</sub>	...	318.32/267	28.70 <sup>+4.04</sup> <sub>-3.48</sub>	320.56/267
	BAT <sup>T</sup>	4.57 <sup>+0.85</sup> <sub>-0.76</sub>	14.63 <sup>+3.18</sup> <sub>-2.25</sub>	7.07/9	-2.46 <sup>+0.14</sup> <sub>-0.15</sub>	...	9.11/11	28.43 <sup>+4.45</sup> <sub>-3.81</sub>	10.15/11
2	GBM <sup>U</sup>	7.45 <sup>+0.57</sup> <sub>-0.57</sub>	...	283.25/266	-2.37 <sup>+0.12</sup> <sub>-0.13</sub>	...	274.28/266	25.06 <sup>+3.80</sup> <sub>-3.19</sub>	268.61/266
	BAT <sup>T</sup>	4.07 <sup>+1.32</sup> <sub>-1.18</sub>	13.17 <sup>+3.12</sup> <sub>-2.13</sub>	2.39/7	-2.40 <sup>+0.15</sup> <sub>-0.16</sub>	...	4.21/9	30.15 <sup>+5.23</sup> <sub>-4.36</sub>	3.51/9
3	BAT <sup>T</sup>	...	...	...	-1.56 <sup>+0.35</sup> <sub>-0.35</sub>	...	4.09/2	...	...
4	BAT <sup>T</sup>	3.05 <sup>+0.92</sup> <sub>-0.84</sub>	10.07 <sup>+2.30</sup> <sub>-1.94</sub>	11.43/9	-3.29 <sup>+0.31</sup> <sub>-0.37</sub>	...	14.53/11	15.78 <sup>+4.21</sup> <sub>-3.56</sub>	14.03/11
5	BAT <sup>T</sup>	3.56 <sup>+1.11</sup> <sub>-0.91</sub>	10.00 <sup>+1.92</sup> <sub>-1.13</sub>	14.27/13	-2.81 <sup>+0.11</sup> <sub>-0.11</sub>	...	20.84/17	21.23 <sup>+1.95</sup> <sub>-1.79</sub>	14.80/15
6	GBM <sup>U</sup>	5.70 <sup>+0.73</sup> <sub>-0.65</sub>	...	173.25/197	-2.48 <sup>+0.22</sup> <sub>-0.24</sub>	...	178.00/197	...	...
7	GBM <sup>U</sup>	7.63 <sup>+0.39</sup> <sub>-0.38</sub>	...	219.02/199	0.02 <sup>+0.55</sup> <sub>-0.49</sub>	29.27 <sup>+2.00</sup> <sub>-2.00</sub>	211.97/198	26.48 <sup>+2.62</sup> <sub>-2.34</sub>	216.84/199
8	GBM <sup>U</sup>	4.80 <sup>+1.00</sup> <sub>-0.81</sub>	17.90 <sup>+4.34</sup> <sub>-3.18</sub>	327.14/330	-2.20 <sup>+0.15</sup> <sub>-0.15</sub>	...	333.04/332	36.71 <sup>+8.32</sup> <sub>-6.67</sub>	329.76/332
9	GBM <sup>U</sup>	3.65 <sup>+0.63</sup> <sub>-0.54</sub>	14.23 <sup>+1.39</sup> <sub>-1.20</sub>	377.46/326	-2.07 <sup>+0.08</sup> <sub>-0.08</sub>	...	399.60/328	42.21 <sup>+4.81</sup> <sub>-4.25</sub>	381.17/328
10	GBM <sup>T</sup>	4.86 <sup>+0.70</sup> <sub>-0.67</sub>	11.87 <sup>+1.77</sup> <sub>-1.27</sub>	206.28/194	-0.46 <sup>+0.30</sup> <sub>-0.28</sub>	30.08 <sup>+1.64</sup> <sub>-1.71</sub>	207.11/195	27.97 <sup>+1.83</sup> <sub>-1.69</sub>	210.93/196
11	GBM <sup>U</sup>	7.44 <sup>+0.82</sup> <sub>-0.73</sub>	...	170.04/197	-2.36 <sup>+0.18</sup> <sub>-0.15</sub>	...	190.88/197	26.23 <sup>+5.10</sup> <sub>-4.54</sub>	175.47/197
12	GBM <sup>T</sup>	4.61 <sup>+0.81</sup> <sub>-0.90</sub>	9.44 <sup>+1.26</sup> <sub>-0.87</sub>	178.18/197	0.15 <sup>+0.32</sup> <sub>-0.31</sub>	27.45 <sup>+1.15</sup> <sub>-1.20</sub>	178.68/198	23.22 <sup>+1.32</sup> <sub>-1.28</sub>	194.46/199
13	GBM <sup>U</sup>	3.51 <sup>+0.78</sup> <sub>-1.11</sub>	11.89 <sup>+2.08</sup> <sub>-2.02</sub>	232.10/195	-2.33 <sup>+0.11</sup> <sub>-0.12</sub>	...	242.03/197	28.51 <sup>+4.25</sup> <sub>-3.65</sub>	233.83/197
14	GBM <sup>U</sup>	7.60 <sup>+1.19</sup> <sub>-1.26</sub>	...	276.25/330	-2.27 <sup>+0.15</sup> <sub>-0.17</sub>	...	268.81/330	30.42 <sup>+6.77</sup> <sub>-5.41</sub>	265.19/330
15	GBM <sup>U</sup>	3.39 <sup>+0.80</sup> <sub>-0.65</sub>	13.56 <sup>+1.61</sup> <sub>-1.35</sub>	331.35/333	-2.11 <sup>+0.10</sup> <sub>-0.11</sub>	...	346.00/335	39.92 <sup>+6.16</sup> <sub>-5.25</sub>	334.94/335
16	GBM <sup>T</sup>	4.41 <sup>+0.69</sup> <sub>-0.63</sub>	10.05 <sup>+0.50</sup> <sub>-0.39</sub>	129.42/127	0.37 <sup>+0.18</sup> <sub>-0.17</sub>	32.96 <sup>+0.70</sup> <sub>-0.70</sub>	131.45/128	28.75 <sup>+0.94</sup> <sub>-0.96</sub>	209.86/129
17	GBM <sup>U</sup>	6.57 <sup>+0.60</sup> <sub>-0.55</sub>	...	190.57/199	-2.39 <sup>+0.13</sup> <sub>-0.14</sub>	...	190.89/199	24.24 <sup>+4.56</sup> <sub>-3.79</sub>	184.59/199
18	GBM <sup>T</sup>	4.85 <sup>+0.42</sup> <sub>-0.42</sub>	19.74 <sup>+1.83</sup> <sub>-1.68</sub>	417.55/327	-2.19 <sup>+0.05</sup> <sub>-0.05</sub>	...	421.37/329	39.84 <sup>+3.10</sup> <sub>-2.77</sub>	424.40/329
19	GBM <sup>T</sup>	6.57 <sup>+0.48</sup> <sub>-1.12</sub>	12.11 <sup>+2.30</sup> <sub>-2.17</sub>	232.47/198	0.49 <sup>+0.20</sup> <sub>-0.19</sub>	30.76 <sup>+0.67</sup> <sub>-0.67</sub>	232.25/199	26.72 <sup>+0.94</sup> <sub>-0.87</sub>	308.87/200

**Table 5** continued on next page



Table 5 (continued)

ID	Instrument	BB+BB or BB		COMPT or PL		OTTB			
		kT <sub>1</sub> (keV)	kT <sub>2</sub> (keV)	χ <sup>2</sup> / <i>d.o.f</i>	Γ	kT (keV)	χ <sup>2</sup> / <i>d.o.f</i>	kT (keV)	χ <sup>2</sup> / <i>d.o.f</i>
20	GBM <sup>U</sup>	3.55 <sup>+0.80</sup> <sub>-0.63</sub>	12.12 <sup>+1.56</sup> <sub>-1.22</sub>	140.14/130	-2.24 <sup>+0.11</sup> <sub>-0.11</sub>	...	158.25/132	32.32 <sup>+4.56</sup> <sub>-3.87</sub>	143.37/132
21	GBM <sup>T</sup>	3.55 <sup>+0.73</sup> <sub>-0.64</sub>	9.81 <sup>+0.85</sup> <sub>-0.68</sub>	199.67/195	-0.26 <sup>+0.36</sup> <sub>-0.34</sub>	29.56 <sup>+1.75</sup> <sub>-1.82</sub>	202.00/196	26.73 <sup>+2.02</sup> <sub>-1.87</sub>	207.12/197
22	GBM <sup>T</sup>	8.98 <sup>+0.70</sup> <sub>-0.69</sub>	...	307.36/265	-2.20 <sup>+0.11</sup> <sub>-0.11</sub>	...	305.31/265	33.39 <sup>+5.28</sup> <sub>-4.41</sub>	296.89/265
23	GBM <sup>T</sup>	4.13 <sup>+0.78</sup> <sub>-0.72</sub>	12.08 <sup>+1.71</sup> <sub>-1.36</sub>	256.93/261	-2.38 <sup>+0.10</sup> <sub>-0.12</sub>	...	278.78/263	28.39 <sup>+3.67</sup> <sub>-3.12</sub>	259.94/263
24	GBM <sup>T</sup>	5.36 <sup>+0.42</sup> <sub>-0.41</sub>	16.50 <sup>+1.74</sup> <sub>-1.50</sub>	133.32/129	-1.00 <sup>+0.22</sup> <sub>-0.21</sub>	33.42 <sup>+2.42</sup> <sub>-2.57</sub>	138.01/130	33.42 <sup>+2.27</sup> <sub>-2.10</sub>	138.01/131
25	GBM <sup>T</sup>	4.37 <sup>+0.75</sup> <sub>-0.72</sub>	9.58 <sup>+0.68</sup> <sub>-0.52</sub>	223.61/193	0.31 <sup>+0.23</sup> <sub>-0.22</sub>	30.72 <sup>+0.83</sup> <sub>-0.83</sub>	224.89/194	26.73 <sup>+1.10</sup> <sub>-1.02</sub>	269.07/195
26	GBM <sup>T</sup>	3.77 <sup>+0.97</sup> <sub>-0.85</sub>	8.75 <sup>+0.50</sup> <sub>-0.35</sub>	351.30/260	0.53 <sup>+0.21</sup> <sub>-0.20</sub>	29.99 <sup>+0.66</sup> <sub>-0.66</sub>	351.52/261	25.47 <sup>+0.87</sup> <sub>-0.86</sub>	422.19/262
27	GBM <sup>T</sup>	4.16 <sup>+0.75</sup> <sub>-0.71</sub>	10.14 <sup>+1.02</sup> <sub>-0.75</sub>	199.18/195	-0.23 <sup>+0.29</sup> <sub>-0.28</sub>	29.60 <sup>+1.36</sup> <sub>-1.40</sub>	199.56/196	26.84 <sup>+1.64</sup> <sub>-1.50</sub>	207.74/197
28	GBM <sup>T</sup>	4.37 <sup>+0.52</sup> <sub>-0.52</sub>	12.05 <sup>+1.30</sup> <sub>-1.09</sub>	177.90/197	-0.81 <sup>+0.30</sup> <sub>-0.29</sub>	28.73 <sup>+2.23</sup> <sub>-2.50</sub>	178.90/198	27.70 <sup>+2.12</sup> <sub>-1.92</sub>	179.34/199
29	GBM <sup>T</sup>	8.55 <sup>+0.48</sup> <sub>-0.46</sub>	...	277.40/268	-2.24 <sup>+0.08</sup> <sub>-0.09</sub>	...	296.89/268	30.95 <sup>+3.44</sup> <sub>-3.02</sub>	269.35/268
30	GBM <sup>U</sup>	8.28 <sup>+1.33</sup> <sub>-1.37</sub>	...	377.01/333	-2.41 <sup>+0.17</sup> <sub>-0.19</sub>	...	369.70/333	28.33 <sup>+6.62</sup> <sub>-5.41</sub>	366.73/333
31	GBM <sup>U</sup>	10.31 <sup>+1.26</sup> <sub>-1.08</sub>	...	181.53/201	-2.04 <sup>+0.14</sup> <sub>-0.14</sub>	...	180.84/201	43.13 <sup>+9.24</sup> <sub>-7.26</sub>	172.53/201
32	GBM <sup>T</sup>	5.43 <sup>+0.59</sup> <sub>-0.55</sub>	15.41 <sup>+3.59</sup> <sub>-2.58</sub>	172.01/196	-2.33 <sup>+0.08</sup> <sub>-0.08</sub>	...	209.73/198	27.29 <sup>+2.65</sup> <sub>-2.37</sub>	179.55/198
	BAT <sup>T</sup>	4.05 <sup>+1.03</sup> <sub>-1.06</sub>	12.16 <sup>+2.98</sup> <sub>-2.30</sub>	11.53/15	-3.01 <sup>+0.23</sup> <sub>-0.25</sub>	...	13.65/17	19.06 <sup>+4.20</sup> <sub>-3.44</sub>	13.53/17
33	GBM <sup>U</sup>	10.19 <sup>+1.17</sup> <sub>-1.07</sub>	...	214.76/198	-2.03 <sup>+0.13</sup> <sub>-0.14</sub>	...	209.96/198	43.26 <sup>+9.41</sup> <sub>-7.60</sub>	203.55/198
34	GBM <sup>T</sup>	9.94 <sup>+0.75</sup> <sub>-0.71</sub>	...	159.30/133	-2.06 <sup>+0.09</sup> <sub>-0.11</sub>	...	180.63/133	38.40 <sup>+6.00</sup> <sub>-4.71</sub>	159.96/133
35	BAT <sup>U</sup>	9.87 <sup>+4.70</sup> <sub>-2.34</sub>	...	1.35/1	-1.94 <sup>+0.44</sup> <sub>-0.49</sub>	...	0.02/1	48.82 <sup>+58.15</sup> <sub>-21.59</sub>	0.11/1
36	GBM <sup>T</sup>	5.60 <sup>+0.35</sup> <sub>-0.35</sub>	10.15 <sup>+0.28</sup> <sub>-0.23</sub>	539.46/330	0.70 <sup>+0.06</sup> <sub>-0.06</sub>	33.03 <sup>+0.21</sup> <sub>-0.21</sub>	541.21/331	27.86 <sup>+0.31</sup> <sub>-0.28</sub>	1533.10/332
	BAT <sup>T</sup>	6.47 <sup>+0.64</sup> <sub>-0.96</sub>	11.02 <sup>+1.86</sup> <sub>-1.22</sub>	36.93/29	0.13 <sup>+0.19</sup> <sub>-0.19</sub>	27.38 <sup>+0.90</sup> <sub>-0.97</sub>	35.17/30	19.26 <sup>+0.29</sup> <sub>-0.29</sub>	78.21/31
37	GBM <sup>T</sup>	8.06 <sup>+0.76</sup> <sub>-0.74</sub>	...	129.41/131	-2.25 <sup>+0.12</sup> <sub>-0.14</sub>	...	139.74/131	29.30 <sup>+5.03</sup> <sub>-4.09</sub>	125.61/131
38	GBM <sup>T</sup>	5.22 <sup>+0.53</sup> <sub>-0.57</sub>	11.97 <sup>+1.49</sup> <sub>-1.17</sub>	211.32/198	-0.24 <sup>+0.24</sup> <sub>-0.23</sub>	29.85 <sup>+1.16</sup> <sub>-1.17</sub>	213.83/199	27.21 <sup>+1.39</sup> <sub>-1.28</sub>	226.49/200
39	GBM <sup>T</sup>	6.44 <sup>+0.54</sup> <sub>-0.65</sub>	14.19 <sup>+2.65</sup> <sub>-1.89</sub>	149.70/130	-0.01 <sup>+0.22</sup> <sub>-0.21</sub>	32.56 <sup>+1.02</sup> <sub>-1.01</sub>	151.78/131	29.69 <sup>+1.37</sup> <sub>-1.25</sub>	177.74/132
40	GBM <sup>T</sup>	6.08 <sup>+0.47</sup> <sub>-0.45</sub>	...	211.57/198	-2.44 <sup>+0.11</sup> <sub>-0.11</sub>	...	213.59/198	23.71 <sup>+3.49</sup> <sub>-3.06</sub>	202.63/198

Table 5 continued on next page

Table 5 (continued)

ID	Instrument	BB+BB or BB		COMPT or PL		OTTB			
		kT <sub>1</sub> (keV)	kT <sub>2</sub> (keV)	$\chi^2/d.o.f$	$\Gamma$	kT (keV)	$\chi^2/d.o.f$	kT (keV)	$\chi^2/d.o.f$
41	GBM <sup>T</sup>	5.38 <sup>+0.48</sup> <sub>-0.47</sub>	17.48 <sup>+1.98</sup> <sub>-1.68</sub>	360.07/333	-1.09 <sup>+0.23</sup> <sub>-0.22</sub>	37.81 <sup>+3.18</sup> <sub>-3.19</sub>	363.13/334	38.10 <sup>+3.01</sup> <sub>-2.74</sub>	363.27/335
42	GBM <sup>U</sup>	12.46 <sup>+1.30</sup> <sub>-1.18</sub>	...	407.12/335	-2.00 <sup>+0.15</sup> <sub>-0.15</sub>	...	419.40/335	...	...
43	GBM <sup>U</sup>	5.21 <sup>+0.99</sup> <sub>-1.06</sub>	15.51 <sup>+5.52</sup> <sub>-3.56</sub>	243.26/264	-2.33 <sup>+0.12</sup> <sub>-0.12</sub>	...	252.42/266	28.91 <sup>+4.36</sup> <sub>-3.71</sub>	242.90/266
44	GBM <sup>T</sup>	8.74 <sup>+0.40</sup> <sub>-0.39</sub>	...	233.94/197	-0.17 <sup>+0.41</sup> <sub>-0.37</sub>	34.66 <sup>+2.18</sup> <sub>-2.05</sub>	220.34/196	33.60 <sup>+3.00</sup> <sub>-2.73</sub>	226.05/197
45	GBM <sup>U</sup>	7.37 <sup>+0.78</sup> <sub>-0.74</sub>	...	141.28/131	-2.32 <sup>+0.16</sup> <sub>-0.14</sub>	...	151.95/131	26.55 <sup>+5.22</sup> <sub>-4.23</sub>	139.78/131
46	GBM <sup>T</sup>	7.08 <sup>+0.44</sup> <sub>-0.43</sub>	...	214.49/200	-2.44 <sup>+0.09</sup> <sub>-0.11</sub>	...	235.33/200	23.67 <sup>+2.73</sup> <sub>-2.38</sub>	208.75/200
47	GBM <sup>U</sup>	9.17 <sup>+1.01</sup> <sub>-0.94</sub>	...	201.48/200	-2.27 <sup>+0.15</sup> <sub>-0.18</sub>	...	207.48/200	30.43 <sup>+6.52</sup> <sub>-5.03</sub>	198.08/200
	BAT <sup>T</sup>	9.03 <sup>+1.49</sup> <sub>-1.44</sub>	...	10.85/7	-2.62 <sup>+0.34</sup> <sub>-0.41</sub>	...	11.88/7	25.45 <sup>+8.90</sup> <sub>-6.71</sub>	10.53/7
48	GBM <sup>U</sup>	7.04 <sup>+0.87</sup> <sub>-0.89</sub>	...	311.28/330	-2.51 <sup>+0.15</sup> <sub>-0.17</sub>	...	302.87/330	24.19 <sup>+4.79</sup> <sub>-3.98</sub>	299.58/330
49	GBM <sup>U</sup>	5.09 <sup>+0.77</sup> <sub>-0.74</sub>	18.29 <sup>+3.21</sup> <sub>-2.59</sub>	357.22/330	-2.20 <sup>+0.09</sup> <sub>-0.10</sub>	...	366.02/332	37.97 <sup>+5.18</sup> <sub>-4.45</sub>	358.80/332
50	GBM <sup>T</sup>	5.75 <sup>+0.61</sup> <sub>-0.74</sub>	11.79 <sup>+1.73</sup> <sub>-1.27</sub>	323.18/330	0.05 <sup>+0.23</sup> <sub>-0.22</sub>	30.53 <sup>+0.95</sup> <sub>-0.96</sub>	323.35/331	26.72 <sup>+1.17</sup> <sub>-1.07</sub>	349.87/332
51	GBM <sup>U</sup>	9.00 <sup>+0.94</sup> <sub>-0.87</sub>	...	233.13/198	-2.11 <sup>+0.12</sup> <sub>-0.14</sub>	...	237.70/198	36.35 <sup>+7.54</sup> <sub>-6.16</sub>	229.37/198
52	GBM <sup>U</sup>	3.26 <sup>+0.67</sup> <sub>-0.53</sub>	13.45 <sup>+2.92</sup> <sub>-2.32</sub>	132.07/128	-2.43 <sup>+0.19</sup> <sub>-0.20</sub>	...	136.51/130	25.84 <sup>+6.38</sup> <sub>-5.27</sub>	136.21/130
53	GBM <sup>T</sup>	7.39 <sup>+0.24</sup> <sub>-0.27</sub>	13.70 <sup>+0.92</sup> <sub>-0.79</sub>	347.54/264	...	...	...	30.86 <sup>+0.46</sup> <sub>-0.42</sub>	959.44/266
54	GBM <sup>T</sup>	6.63 <sup>+0.55</sup> <sub>-0.64</sub>	12.43 <sup>+1.66</sup> <sub>-1.13</sub>	279.38/263	0.35 <sup>+0.12</sup> <sub>-0.12</sub>	33.32 <sup>+0.48</sup> <sub>-0.48</sub>	276.85/264	29.29 <sup>+0.64</sup> <sub>-0.65</sub>	439.20/265
55	GBM <sup>T</sup>	7.11 <sup>+0.29</sup> <sub>-0.30</sub>	15.66 <sup>+0.99</sup> <sub>-0.86</sub>	184.96/127	0.07 <sup>+0.10</sup> <sub>-0.09</sub>	38.30 <sup>+0.55</sup> <sub>-0.54</sub>	204.12/128	36.45 <sup>+0.80</sup> <sub>-0.79</sub>	368.24/129
56	GBM <sup>T</sup>	4.25 <sup>+0.79</sup> <sub>-0.75</sub>	9.29 <sup>+1.15</sup> <sub>-0.76</sub>	190.65/197	-0.03 <sup>+0.31</sup> <sub>-0.30</sub>	26.96 <sup>+1.16</sup> <sub>-1.21</sub>	190.89/198	23.41 <sup>+1.32</sup> <sub>-1.24</sub>	202.77/199
57	GBM <sup>T</sup>	4.71 <sup>+0.55</sup> <sub>-0.54</sub>	9.73 <sup>+0.75</sup> <sub>-0.56</sub>	170.02/130	0.20 <sup>+0.18</sup> <sub>-0.17</sub>	29.10 <sup>+0.63</sup> <sub>-0.63</sub>	170.81/131	25.61 <sup>+0.80</sup> <sub>-0.80</sub>	231.21/132
58	BAT <sup>T</sup>	7.79 <sup>+1.22</sup> <sub>-1.10</sub>	...	6.17/5	-2.68 <sup>+0.40</sup> <sub>-0.40</sub>	...	10.64/5	22.06 <sup>+6.71</sup> <sub>-5.08</sub>	7.53/5
59	BAT <sup>U</sup>	5.68 <sup>+1.76</sup> <sub>-1.76</sub>	...	2.37/1	-2.54 <sup>+0.82</sup> <sub>-1.32</sub>	...	1.49/1	...	...
60	BAT <sup>U</sup>	7.57 <sup>+1.88</sup> <sub>-1.35</sub>	...	0.32/1	-2.50 <sup>+0.44</sup> <sub>-0.53</sub>	...	0.33/1	24.82 <sup>+14.38</sup> <sub>-8.38</sub>	0.00/1
61	BAT <sup>U</sup>	...	...	...	-1.46 <sup>+0.58</sup> <sub>-0.62</sub>	...	0.01 / 2	...	...
62	BAT <sup>U</sup>	9.47 <sup>+3.51</sup> <sub>-3.51</sub>	...	2.58/1	-1.47 <sup>+0.84</sup> <sub>-0.85</sub>	...	0.65/1	...	...

Table 5 continued on next page

Table 5 (continued)

ID	Instrument	BB+BB or BB		COMPT or PL		OTTB			
		kT <sub>1</sub> (keV)	kT <sub>2</sub> (keV)	χ <sup>2</sup> / <i>d.o.f</i>	Γ	kT (keV)	χ <sup>2</sup> / <i>d.o.f</i>	kT (keV)	χ <sup>2</sup> / <i>d.o.f</i>
63	BAT <sup>T</sup>	5.24 <sup>+1.12</sup> <sub>-1.01</sub>	14.79 <sup>+3.63</sup> <sub>-2.34</sub>	11.74/6	-2.41 <sup>+0.12</sup> <sub>-0.12</sub>	...	15.83/8	30.36 <sup>+3.83</sup> <sub>-3.35</sub>	12.63/8
64	GBM <sup>T</sup>	6.32 <sup>+0.40</sup> <sub>-0.45</sub>	13.70 <sup>+2.22</sup> <sub>-1.65</sub>	295.03/196	0.22 <sup>+0.19</sup> <sub>-0.19</sub>	31.00 <sup>+0.72</sup> <sub>-0.71</sub>	303.61/197	28.43 <sup>+0.99</sup> <sub>-0.97</sub>	357.36/198
65	GBM <sup>T</sup>	5.22 <sup>+0.72</sup> <sub>-0.71</sub>	13.64 <sup>+3.10</sup> <sub>-2.07</sub>	417.07/332	-2.37 <sup>+0.07</sup> <sub>-0.08</sub>	...	450.50/334	27.21 <sup>+2.48</sup> <sub>-2.24</sub>	419.73/334
66	GBM <sup>T</sup>	4.86 <sup>+0.59</sup> <sub>-0.70</sub>	10.08 <sup>+1.05</sup> <sub>-0.82</sub>	321.39/329	0.03 <sup>+0.24</sup> <sub>-0.23</sub>	28.12 <sup>+0.94</sup> <sub>-0.97</sub>	321.96/330	23.91 <sup>+1.01</sup> <sub>-0.99</sub>	345.24/331
67	GBM <sup>U</sup>	8.54 <sup>+1.34</sup> <sub>-1.24</sub>	...	197.88/197	-2.28 <sup>+0.21</sup> <sub>-0.25</sub>	...	197.33/197	...	...
68	GBM <sup>U</sup>	5.23 <sup>+0.52</sup> <sub>-0.48</sub>	20.99 <sup>+3.40</sup> <sub>-2.77</sub>	75.22/63	-2.08 <sup>+0.09</sup> <sub>-0.09</sub>	...	91.78/65	38.90 <sup>+5.27</sup> <sub>-4.51</sub>	85.39/65
69	GBM <sup>T</sup>	4.94 <sup>+0.90</sup> <sub>-0.78</sub>	15.19 <sup>+2.45</sup> <sub>-1.72</sub>	254.74/195	-2.11 <sup>+0.07</sup> <sub>-0.07</sub>	...	273.33/197	39.06 <sup>+3.98</sup> <sub>-3.53</sub>	253.36/197
70	GBM <sup>U</sup>	9.96 <sup>+0.95</sup> <sub>-0.90</sub>	...	336.27/330	-2.06 <sup>+0.13</sup> <sub>-0.13</sub>	...	334.52/330	40.29 <sup>+7.81</sup> <sub>-6.32</sub>	326.89/330
71	GBM <sup>U</sup>	10.22 <sup>+0.77</sup> <sub>-0.75</sub>	...	174.59/202	-2.12 <sup>+0.11</sup> <sub>-0.11</sub>	...	183.05/202	37.97 <sup>+5.83</sup> <sub>-4.75</sub>	165.91/202
72	GBM <sup>T</sup>	5.69 <sup>+0.49</sup> <sub>-0.51</sub>	10.18 <sup>+0.66</sup> <sub>-0.49</sub>	227.52/201	0.61 <sup>+0.11</sup> <sub>-0.11</sub>	31.27 <sup>+0.37</sup> <sub>-0.37</sub>	230.08/202	26.96 <sup>+0.54</sup> <sub>-0.51</sub>	514.77/203
73	GBM <sup>T</sup>	6.41 <sup>+0.32</sup> <sub>-0.32</sub>	11.26 <sup>+0.35</sup> <sub>-0.29</sub>	366.23/202	0.70 <sup>+0.05</sup> <sub>-0.05</sub>	35.45 <sup>+0.20</sup> <sub>-0.20</sub>	368.83/203	31.46 <sup>+0.32</sup> <sub>-0.29</sub>	1831.80/204
74	GBM <sup>T</sup>	4.99 <sup>+0.78</sup> <sub>-0.80</sub>	12.26 <sup>+2.48</sup> <sub>-1.66</sub>	360.91/333	-0.54 <sup>+0.35</sup> <sub>-0.32</sub>	29.72 <sup>+1.92</sup> <sub>-2.02</sub>	360.86/334	28.00 <sup>+2.13</sup> <sub>-1.95</sub>	363.01/335
75	BAT <sup>U</sup>	15.10 <sup>+3.41</sup> <sub>-2.78</sub>	...	0.34/2	-1.52 <sup>+0.35</sup> <sub>-0.37</sub>	...	1.26/2	...	...
76	BAT <sup>T</sup>	6.18 <sup>+0.71</sup> <sub>-0.92</sub>	11.46 <sup>+3.04</sup> <sub>-1.76</sub>	21.63/23	0.11 <sup>+0.44</sup> <sub>-0.41</sub>	27.19 <sup>+1.55</sup> <sub>-1.87</sub>	23.20/24	20.56 <sup>+0.85</sup> <sub>-0.81</sub>	31.61/25
77	BAT <sup>U</sup>	10.00 <sup>+0.97</sup> <sub>-0.90</sub>	...	5.83/4	-2.25 <sup>+0.17</sup> <sub>-0.18</sub>	...	3.24/4	34.78 <sup>+7.18</sup> <sub>-5.64</sub>	0.88/4
78	BAT <sup>U</sup>	9.60 <sup>+0.53</sup> <sub>-0.51</sub>	...	6.71/5	-0.29 <sup>+0.82</sup> <sub>-0.70</sub>	34.76 <sup>+3.16</sup> <sub>-4.66</sub>	2.27/4	30.80 <sup>+3.43</sup> <sub>-3.02</sub>	3.30/5
79	GBM <sup>T</sup>	5.50 <sup>+0.78</sup> <sub>-0.66</sub>	17.88 <sup>+6.76</sup> <sub>-3.60</sub>	234.02/196	-2.20 <sup>+0.08</sup> <sub>-0.08</sub>	...	250.16/198	30.62 <sup>+3.65</sup> <sub>-3.22</sub>	237.16/198
80	GBM <sup>U</sup>	3.76 <sup>+0.61</sup> <sub>-0.58</sub>	9.60 <sup>+0.74</sup> <sub>-0.59</sub>	228.58/198	-0.26 <sup>+0.26</sup> <sub>-0.24</sub>	28.56 <sup>+1.19</sup> <sub>-1.23</sub>	228.80/199	25.70 <sup>+1.32</sup> <sub>-1.26</sub>	238.95/200
81	GBM <sup>U</sup>	4.31 <sup>+0.80</sup> <sub>-0.73</sub>	16.25 <sup>+3.86</sup> <sub>-3.10</sub>	206.30/194	-2.33 <sup>+0.14</sup> <sub>-0.16</sub>	...	211.05/196	30.23 <sup>+6.52</sup> <sub>-5.40</sub>	208.39/196
82	GBM <sup>T</sup>	5.41 <sup>+0.42</sup> <sub>-0.42</sub>	11.94 <sup>+1.02</sup> <sub>-0.82</sub>	381.06/336	-0.16 <sup>+0.16</sup> <sub>-0.15</sub>	30.61 <sup>+0.74</sup> <sub>-0.75</sub>	383.50/337	27.50 <sup>+0.85</sup> <sub>-0.83</sub>	418.13/338
83	GBM <sup>T</sup>	3.79 <sup>+0.51</sup> <sub>-0.47</sub>	11.11 <sup>+1.18</sup> <sub>-0.94</sub>	148.57/130	-2.27 <sup>+0.06</sup> <sub>-0.06</sub>	...	175.59/132	27.46 <sup>+2.22</sup> <sub>-2.01</sub>	148.83/132
84	GBM <sup>U</sup>	10.93 <sup>+2.38</sup> <sub>-2.13</sub>	...	138.85/135	-1.96 <sup>+0.19</sup> <sub>-0.21</sub>	...	129.67/135	...	...
85	GBM <sup>U</sup>	9.29 <sup>+0.94</sup> <sub>-0.88</sub>	...	225.53/202	-2.13 <sup>+0.13</sup> <sub>-0.15</sub>	...	228.08/202	34.45 <sup>+7.34</sup> <sub>-5.81</sub>	220.79/202

Table 5 continued on next page

Table 5 (continued)

ID	Instrument	BB+BB or BB		COMPT or PL		OTTB			
		kT <sub>1</sub> (keV)	kT <sub>2</sub> (keV)	χ <sup>2</sup> /d.o.f	Γ	kT (keV)	χ <sup>2</sup> /d.o.f	kT (keV)	χ <sup>2</sup> /d.o.f
86	GBM <sup>U</sup>	6.72 <sup>+1.06</sup> <sub>-0.96</sub>	...	201.41/205	-2.22 <sup>+0.16</sup> <sub>-0.17</sub>	...	196.19/205	29.83 <sup>+7.89</sup> <sub>-6.28</sub>	192.26/204
87	GBM <sup>U</sup>	4.18 <sup>+0.61</sup> <sub>-0.54</sub>	17.51 <sup>+4.06</sup> <sub>-3.11</sub>	136.27/129	-2.30 <sup>+0.14</sup> <sub>-0.15</sub>	...	142.08/131	28.83 <sup>+6.44</sup> <sub>-5.49</sub>	142.05/131
88	GBM <sup>T</sup>	6.91 <sup>+0.61</sup> <sub>-1.03</sub>	11.99 <sup>+2.78</sup> <sub>-1.83</sub>	197.85/195	0.70 <sup>+0.20</sup> <sub>-0.20</sub>	32.19 <sup>+0.65</sup> <sub>-0.65</sub>	198.83/196	27.85 <sup>+0.92</sup> <sub>-0.94</sub>	299.44/197
89	GBM <sup>U</sup>	8.28 <sup>+1.22</sup> <sub>-1.13</sub>	...	172.49/130	-1.92 <sup>+0.13</sup> <sub>-0.14</sub>	...	153.13/130	51.43 <sup>+15.10</sup> <sub>-11.10</sub>	156.53/130
90	GBM <sup>T</sup>	4.21 <sup>+0.98</sup> <sub>-0.94</sub>	12.86 <sup>+2.52</sup> <sub>-1.89</sub>	144.32/130	-2.21 <sup>+0.09</sup> <sub>-0.10</sub>	...	157.64/132	31.62 <sup>+4.25</sup> <sub>-3.69</sub>	143.76/132
91	GBM <sup>U</sup>	5.69 <sup>+1.05</sup> <sub>-0.84</sub>	...	154.85/131	-2.03 <sup>+0.17</sup> <sub>-0.19</sub>	...	145.69/131	...	...
92	GBM <sup>T</sup>	5.37 <sup>+0.49</sup> <sub>-0.50</sub>	13.15 <sup>+2.59</sup> <sub>-1.75</sub>	238.10/197	-0.41 <sup>+0.26</sup> <sub>-0.24</sub>	26.88 <sup>+1.15</sup> <sub>-1.22</sub>	243.80/198	24.60 <sup>+1.24</sup> <sub>-1.17</sub>	250.20/199
93	GBM <sup>T</sup>	5.52 <sup>+0.60</sup> <sub>-0.69</sub>	10.01 <sup>+1.05</sup> <sub>-0.74</sub>	310.54/266	0.50 <sup>+0.15</sup> <sub>-0.15</sub>	29.88 <sup>+0.50</sup> <sub>-0.50</sub>	310.34/267	25.87 <sup>+0.70</sup> <sub>-0.65</sub>	439.76/268
94	GBM <sup>U</sup>	4.13 <sup>+0.46</sup> <sub>-0.43</sub>	15.05 <sup>+1.81</sup> <sub>-1.57</sub>	284.07/267	-2.25 <sup>+0.08</sup> <sub>-0.08</sub>	...	303.35/269	31.71 <sup>+3.56</sup> <sub>-3.18</sub>	290.10/269
95	GBM <sup>U</sup>	5.33 <sup>+0.45</sup> <sub>-0.43</sub>	11.33 <sup>+0.92</sup> <sub>-0.68</sub>	341.36/268	0.03 <sup>+0.13</sup> <sub>-0.13</sub>	31.41 <sup>+0.57</sup> <sub>-0.56</sub>	342.63/269	28.83 <sup>+0.74</sup> <sub>-0.73</sub>	423.12/270
96	GBM <sup>U</sup>	7.19 <sup>+0.15</sup> <sub>-0.17</sub>	12.68 <sup>+0.91</sup> <sub>-0.77</sub>	587.07/333	0.86 <sup>+0.05</sup> <sub>-0.05</sub>	31.45 <sup>+0.14</sup> <sub>-0.15</sub>	622.47/334	26.75 <sup>+0.22</sup> <sub>-0.20</sub>	2668.00/335
97	GBM <sup>T</sup>	5.63 <sup>+0.28</sup> <sub>-0.29</sub>	11.96 <sup>+0.72</sup> <sub>-0.61</sub>	385.57/334	-0.02 <sup>+0.11</sup> <sub>-0.11</sub>	30.37 <sup>+0.46</sup> <sub>-0.46</sub>	394.66/335	26.83 <sup>+0.55</sup> <sub>-0.53</sub>	499.88/336
98	GBM <sup>U</sup>	4.49 <sup>+1.06</sup> <sub>-0.88</sub>	12.84 <sup>+2.50</sup> <sub>-1.70</sub>	259.03/197	-2.15 <sup>+0.08</sup> <sub>-0.09</sub>	...	274.42/199	34.90 <sup>+4.56</sup> <sub>-3.94</sub>	259.52/199
99	GBM <sup>U</sup>	4.25 <sup>+1.00</sup> <sub>-0.84</sub>	12.73 <sup>+2.49</sup> <sub>-1.70</sub>	211.42/195	-2.19 <sup>+0.08</sup> <sub>-0.09</sub>	...	229.30/197	33.37 <sup>+3.83</sup> <sub>-3.38</sub>	210.29/197
100	GBM <sup>U</sup>	7.65 <sup>+1.36</sup> <sub>-1.30</sub>	...	106.84/130	-2.34 <sup>+0.21</sup> <sub>-0.26</sub>	...	105.94/130	...	...
101	GBM <sup>T</sup>	3.79 <sup>+0.49</sup> <sub>-0.48</sub>	9.04 <sup>+0.35</sup> <sub>-0.30</sub>	270.03/196	0.33 <sup>+0.17</sup> <sub>-0.16</sub>	29.86 <sup>+0.59</sup> <sub>-0.59</sub>	274.81/197	25.89 <sup>+0.78</sup> <sub>-0.77</sub>	356.24/198
102	GBM <sup>U</sup>	10.37 <sup>+3.22</sup> <sub>-3.35</sub>	...	209.40/198	-2.15 <sup>+0.22</sup> <sub>-0.24</sub>	...	201.15/198	...	...
103	GBM <sup>T</sup>	5.37 <sup>+0.45</sup> <sub>-0.46</sub>	11.85 <sup>+1.22</sup> <sub>-0.96</sub>	229.21/200	-0.02 <sup>+0.20</sup> <sub>-0.19</sub>	30.67 <sup>+0.87</sup> <sub>-0.85</sub>	235.56/201	28.43 <sup>+1.14</sup> <sub>-1.10</sub>	267.58/202
104	GBM <sup>T</sup>	5.56 <sup>+1.15</sup> <sub>-0.98</sub>	14.36 <sup>+3.41</sup> <sub>-2.02</sub>	366.77/329	-0.40 <sup>+0.45</sup> <sub>-0.42</sub>	39.51 <sup>+3.80</sup> <sub>-3.13</sub>	367.68/330	40.48 <sup>+4.93</sup> <sub>-4.28</sub>	369.87/331
105	GBM <sup>T</sup>	4.56 <sup>+0.34</sup> <sub>-0.33</sub>	15.58 <sup>+2.14</sup> <sub>-1.79</sub>	419.61/335	-2.43 <sup>+0.06</sup> <sub>-0.06</sub>	...	435.43/337	24.08 <sup>+1.91</sup> <sub>-1.79</sub>	424.92/337
106	GBM <sup>T</sup>	5.86 <sup>+0.33</sup> <sub>-0.33</sub>	12.94 <sup>+0.71</sup> <sub>-0.60</sub>	758.54/331	-0.05 <sup>+0.11</sup> <sub>-0.10</sub>	35.04 <sup>+0.54</sup> <sub>-0.54</sub>	763.76/332	32.70 <sup>+0.71</sup> <sub>-0.71</sub>	866.36/333
107	GBM <sup>U</sup>	4.31 <sup>+0.77</sup> <sub>-0.63</sub>	16.75 <sup>+3.00</sup> <sub>-2.36</sub>	229.75/198	-2.16 <sup>+0.12</sup> <sub>-0.13</sub>	...	238.59/200	38.55 <sup>+7.56</sup> <sub>-6.22</sub>	233.65/200
108	GBM <sup>T</sup>	7.36 <sup>+0.13</sup> <sub>-0.13</sub>	13.16 <sup>+0.23</sup> <sub>-0.21</sub>	628.40/199	0.60 <sup>+0.02</sup> <sub>-0.02</sub>	38.20 <sup>+0.11</sup> <sub>-0.11</sub>	685.27/200	35.25 <sup>+0.17</sup> <sub>-0.19</sub>	6662.50/201

Table 5 continued on next page

Table 5 (continued)

ID	Instrument	BB+BB or BB			COMPT or PL			OTTB		
		kT <sub>1</sub> (keV)	kT <sub>2</sub> (keV)	$\chi^2/d.o.f$	$\Gamma$	kT (keV)	$\chi^2/d.o.f$	kT (keV)	$\chi^2/d.o.f$	
	BAT <sup>T</sup>	7.49 <sup>+0.26</sup> <sub>-0.28</sub>	13.64 <sup>+0.70</sup> <sub>-0.60</sub>	21.47/34	-0.14 <sup>+0.10</sup> <sub>-0.10</sub>	30.44 <sup>+0.68</sup> <sub>-0.71</sub>	31.98/35	22.55 <sup>+0.20</sup> <sub>-0.20</sub>	115.48/36	
109	BAT <sup>T</sup>	17.04 <sup>+5.20</sup> <sub>-4.07</sub>	...	5.79/4	-1.58 <sup>+0.38</sup> <sub>-0.39</sub>	...	3.57/4	...	...	
110	GBM <sup>T</sup>	9.28 <sup>+0.67</sup> <sub>-0.63</sub>	...	239.93/201	-2.24 <sup>+0.11</sup> <sub>-0.10</sub>	...	261.27/201	33.00 <sup>+4.45</sup> <sub>-3.72</sub>	237.83/201	
111	GBM <sup>U</sup>	5.33 <sup>+0.90</sup> <sub>-0.87</sub>	17.71 <sup>+5.27</sup> <sub>-3.59</sub>	359.95/333	-2.27 <sup>+0.11</sup> <sub>-0.12</sub>	...	369.52/335	31.51 <sup>+5.02</sup> <sub>-4.21</sub>	362.01/335	
112	GBM <sup>U</sup>	7.95 <sup>+0.85</sup> <sub>-0.78</sub>	...	272.35/332	-2.27 <sup>+0.13</sup> <sub>-0.16</sub>	...	282.77/332	29.68 <sup>+5.60</sup> <sub>-4.59</sub>	271.25/332	
113	GBM <sup>U</sup>	3.83 <sup>+0.65</sup> <sub>-0.57</sub>	14.87 <sup>+2.59</sup> <sub>-2.07</sub>	348.93/333	-2.32 <sup>+0.12</sup> <sub>-0.13</sub>	...	357.22/335	30.74 <sup>+5.31</sup> <sub>-4.50</sub>	353.94/335	
114	GBM <sup>T</sup>	5.48 <sup>+0.41</sup> <sub>-0.42</sub>	13.31 <sup>+2.06</sup> <sub>-1.51</sub>	447.11/333	-0.38 <sup>+0.23</sup> <sub>-0.22</sub>	27.50 <sup>+1.03</sup> <sub>-1.08</sub>	454.87/334	25.03 <sup>+1.10</sup> <sub>-1.04</sub>	464.03/335	
115	GBM <sup>U</sup>	5.45 <sup>+0.78</sup> <sub>-0.72</sub>	18.15 <sup>+3.77</sup> <sub>-2.78</sub>	370.20/329	-2.16 <sup>+0.10</sup> <sub>-0.11</sub>	...	382.72/331	37.44 <sup>+5.80</sup> <sub>-4.95</sub>	373.34/331	
116	GBM <sup>U</sup>	8.99 <sup>+1.56</sup> <sub>-1.45</sub>	...	136.05/130	-2.27 <sup>+0.24</sup> <sub>-0.22</sub>	...	140.52/130	...	...	
117	GBM <sup>T</sup>	5.35 <sup>+0.51</sup> <sub>-0.54</sub>	13.70 <sup>+1.74</sup> <sub>-1.42</sub>	211.15/197	-0.59 <sup>+0.29</sup> <sub>-0.27</sub>	30.26 <sup>+1.90</sup> <sub>-2.03</sub>	213.46/198	28.17 <sup>+1.94</sup> <sub>-1.77</sub>	215.80/199	
118	GBM <sup>T</sup>	6.26 <sup>+0.42</sup> <sub>-0.44</sub>	12.03 <sup>+0.68</sup> <sub>-0.56</sub>	433.35/330	0.35 <sup>+0.11</sup> <sub>-0.11</sub>	34.92 <sup>+0.45</sup> <sub>-0.45</sub>	434.64/331	30.56 <sup>+0.64</sup> <sub>-0.59</sub>	643.35/332	
119	GBM <sup>U</sup>	...	...	...	-1.66 <sup>+0.13</sup> <sub>-0.13</sub>	...	245.71/199	47.62 <sup>+20.80</sup> <sub>-2.36</sub>	597.54/199	
120	GBM <sup>U</sup>	8.60 <sup>+1.02</sup> <sub>-0.94</sub>	...	231.65/196	-2.18 <sup>+0.16</sup> <sub>-0.19</sub>	...	242.65/196	...	...	
121	GBM <sup>T</sup>	4.30 <sup>+0.79</sup> <sub>-0.71</sub>	11.02 <sup>+1.81</sup> <sub>-1.29</sub>	235.10/196	-2.28 <sup>+0.08</sup> <sub>-0.09</sub>	...	265.84/198	27.63 <sup>+3.13</sup> <sub>-2.76</sub>	238.87/198	
122	GBM <sup>T</sup>	4.93 <sup>+0.48</sup> <sub>-0.47</sub>	12.81 <sup>+1.22</sup> <sub>-0.99</sub>	346.90/331	-0.70 <sup>+0.21</sup> <sub>-0.20</sub>	30.46 <sup>+1.46</sup> <sub>-1.55</sub>	344.71/332	28.87 <sup>+1.42</sup> <sub>-1.34</sub>	347.16/333	
123	GBM <sup>T</sup>	5.28 <sup>+0.64</sup> <sub>-0.61</sub>	11.44 <sup>+1.64</sup> <sub>-1.17</sub>	118.09/130	0.10 <sup>+0.31</sup> <sub>-0.29</sub>	30.65 <sup>+1.25</sup> <sub>-1.21</sub>	122.22/131	28.28 <sup>+1.66</sup> <sub>-1.61</sub>	139.90/132	
124	GBM <sup>T</sup>	5.51 <sup>+0.51</sup> <sub>-0.54</sub>	9.62 <sup>+0.40</sup> <sub>-0.31</sub>	364.61/199	0.78 <sup>+0.07</sup> <sub>-0.07</sub>	31.80 <sup>+0.21</sup> <sub>-0.21</sub>	360.34/200	27.33 <sup>+0.31</sup> <sub>-0.32</sub>	1333.60/201	
125	GBM <sup>T</sup>	4.46 <sup>+0.67</sup> <sub>-0.63</sub>	11.48 <sup>+1.61</sup> <sub>-1.20</sub>	152.62/130	-2.30 <sup>+0.07</sup> <sub>-0.08</sub>	...	187.96/132	27.76 <sup>+2.56</sup> <sub>-2.28</sub>	156.13/132	
126	GBM <sup>T</sup>	4.55 <sup>+0.44</sup> <sub>-0.43</sub>	13.11 <sup>+1.97</sup> <sub>-1.54</sub>	302.02/264	-2.34 <sup>+0.06</sup> <sub>-0.06</sub>	...	336.74/266	26.01 <sup>+2.19</sup> <sub>-2.00</sub>	296.93/266	
127	GBM <sup>T</sup>	3.57 <sup>+0.56</sup> <sub>-0.52</sub>	10.62 <sup>+1.53</sup> <sub>-1.21</sub>	294.25/267	-2.43 <sup>+0.09</sup> <sub>-0.10</sub>	...	311.48/269	23.39 <sup>+2.59</sup> <sub>-2.32</sub>	296.34/269	

## ACKNOWLEDGMENTS

L.L. acknowledges support from the National Natural Science Foundation of China (grant no. 11703002 and 11543004) and the Fundamental Research Funds for the Central Universities. Y.K acknowledges the support from the Scientific and Technological Research Council of Turkey (TÜBİTAK grant no. 118F344).

*Software:* HEASoft (v624; HEASARC 2014), XSPEC (Arnaud 1996), RMFIT (v40rc1; Mallozzi 2000, Preece 2011), GBMDRM (v2.0)

## APPENDIX

## A. EXPLORING THE GBM LOCATION ACCURACY WITH SGR J1935+2154 BURSTS

The soft spectrum and large number of repeated events make short bursts from magnetars a good database to study the systematic location accuracy of GBM in the soft energy band ( $< 50$  keV). We plot the offset to the SGR J1935+2154 position *v.s.* the burst fluence in Figure 12. Weaker bursts present larger offsets as well as larger statistical uncertainties. Brighter bursts with much smaller statistical uncertainties also show offsets with several degrees, which come from systematic effects. This is also pointed out by a similar study using 21 bursts triggered GBM from SGR J1550–5418 (von Kienlin et al. 2012). We set the inverse of the statistical error as the weight of each burst and calculate the weighted mean of the distance to the known source position as  $\sim 4.4^\circ$ . This systematic offset for the soft band of GBM is close to the result of  $3.7^\circ$  from Connaughton et al. (2015) for Gamma-Ray Bursts in the harder GBM energy band (50–300 keV). We note here, however, that a detailed study of the systematic uncertainties of the GBM location in the soft band should include short bursts from other magnetars as well as a more careful modeling, both of which are not within the scope of this paper.

## REFERENCES

- An, H., & Archibald, R. 2019, *ApJL*, 877, L10  
 Arnaud, K. A. 1996, *Astronomical Data Analysis Software and Systems V*, 17  
 Barthelmy, S. D., Barbier, L. M., Cummings, J. R., et al. 2005, *SSRv*, 120, 143  
 Cheng, B., Epstein, R. I., Guyer, R. A., et al. 1996, *Nature*, 382, 518  
 Collazzi, A. C., Kouveliotou, C., van der Horst, A. J., et al. 2015, *ApJS*, 218, 11  
 Connaughton, V., Briggs, M. S., Goldstein, A., et al. 2015, *ApJS*, 216, 32  
 Coti Zelati, F., Rea, N., Pons, J. A., et al. 2018, *MNRAS*, 474, 961  
 Cummings, J. R. 2014, *GRB Coordinates Network* 16530, 1  
 D’Ai, A., Evans, P. A., Burrows, D. N., et al. 2016, *MNRAS*, 463, 2394  
 Duncan, R. C., & Thompson, C. 1992, *ApJL*, 392, L9  
 Esposito, P., Israel, G. L., Zane, S., et al. 2008, *MNRAS*, 390, L34  
 Esposito, P., Rea, N., & Israel, G. L. 2018, arXiv e-prints, arXiv:1803.05716  
 Frail, D. A., Kulkarni, S. R., & Bloom, J. S. 1999, *Nature*, 398, 127  
 Gavriil, F. P., Kaspi, V. M., & Woods, P. M. 2004, *ApJ*, 607, 959  
 Güver, T., Göğüş, E., & Özel, F. 2011, *MNRAS*, 418, 2773  
 Göğüş, E., Kouveliotou, C., Woods, P. M., et al. 2001, *ApJ*, 558, 228  
 Göğüş, E., Woods, P. M., Kouveliotou, C., et al. 2010, *ApJ*, 722, 899

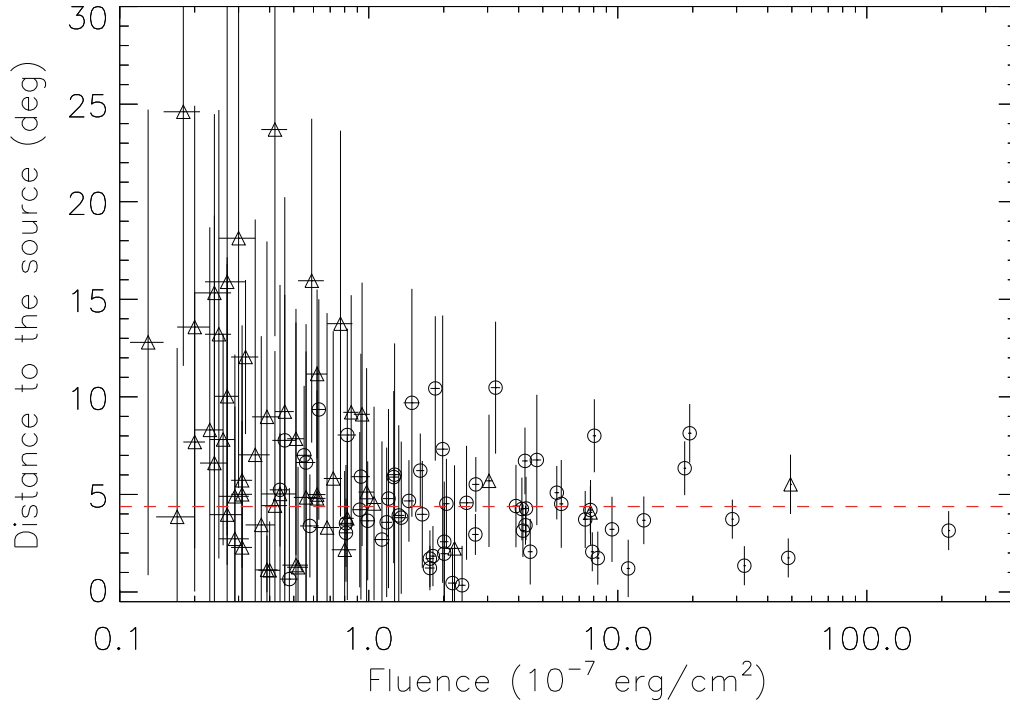


**Figure 12.** The offset of the measured locations to each burst relative to the SGR J1935+2154 position as a function of the burst fluence. The open circles and triangles represent the triggered and un-triggered bursts, respectively. The red dashed line is the weighted average of the offset.

- Gögüş, E. 2014, *Astronomische Nachrichten*, 335, 296
- Gögüş, E., Lin, L., Kaneko, Y., et al. 2016, *ApJL*, 829, L25
- Hurley, K., Cline, T., Mazets, E., et al. 1999, *Nature*, 397, 41
- Hurley, K., Boggs, S. E., Smith, D. M., et al. 2005, *Nature*, 434, 1098
- Israel, G. L., Romano, P., Mangano, V., et al. 2008, *ApJ*, 685, 1114
- Israel, G. L., Esposito, P., Rea, N., et al. 2010, *MNRAS*, 408, 1387
- Israel, G. L., Esposito, P., Rea, N., et al. 2016, *MNRAS*, 457, 3448
- Kaneko, Y., Bostancı, Z. F., Gögüş, E., et al. 2015, *MNRAS*, 452, 824
- Kouveliotou, C., Meegan, C. A., Fishman, G. J., et al. 1993, *ApJL*, 413, L101
- Kouveliotou, C., Dieters, S., Strohmayer, T., et al. 1998, *Nature*, 393, 235
- Kozlova, A. V., Israel, G. L., Svinkin, D. S., et al. 2016, *MNRAS*, 460, 2008
- Lin, L., Kouveliotou, C., Baring, M. G., et al. 2011, *ApJ*, 739, 87
- Lin, L., Kouveliotou, C., Gögüş, E., et al. 2011, *ApJL*, 740, L16
- Lin, L., Gögüş, E., Baring, M. G., et al. 2012, *ApJ*, 756, 54
- Lin, L., Gögüş, E., Kaneko, Y., et al. 2013, *ApJ*, 778, 105
- Lyubarsky, Y., Eichler, D., & Thompson, C. 2002, *ApJL*, 580, L69
- Lytikov, M. 2003, *MNRAS*, 346, 540
- Mazets, E. P., Golentskii, S. V., Ilinskii, V. N., et al. 1979, *Nature*, 282, 587
- Meegan, C., Lichti, G., Bhat, P. N., et al. 2009, *ApJ*, 702, 791
- Norris, J. P., Gehrels, N., & Scargle, J. D. 2010, *ApJ*, 717, 411
- Olausen, S. A., & Kaspi, V. M. 2014, *ApJS*, 212, 6
- Palmer, D. M., Barthelmy, S., Gehrels, N., et al. 2005, *Nature*, 434, 1107
- Rea, N., Israel, G. L., Turolla, R., et al. 2009, *MNRAS*, 396, 2419
- Rea, N., Esposito, P., Turolla, R., et al. 2010, *Science*, 330, 944
- Rea, N., & Esposito, P. 2011, *Astrophysics and Space Science Proceedings*, 21, 247

- Rea, N., Israel, G. L., Esposito, P., et al. 2012, *ApJ*, 754, 27
- Rea, N., Viganò, D., Israel, G. L., et al. 2014, *ApJL*, 781, L17
- Rea, N., Borghese, A., Esposito, P., et al. 2016, *ApJL*, 828, L13
- Scargle, J. D., Norris, J. P., Jackson, B., et al. 2013, *ApJ*, 764, 167
- Thompson, C., & Duncan, R. C. 1995, *MNRAS*, 275, 255
- Tiengo, A., Esposito, P., Mereghetti, S., et al. 2013, *Nature*, 500, 312
- Turolla, R., Zane, S., & Watts, A. L. 2015, *Reports on Progress in Physics*, 78, 116901
- van der Horst, A. J., Kouveliotou, C., Gorgone, N. M., et al. 2012, *ApJ*, 749, 122
- von Kienlin, A., Gruber, D., Kouveliotou, C., et al. 2012, *ApJ*, 755, 150
- Woods, P. M., Kouveliotou, C., van Paradijs, J., et al. 1999, *ApJL*, 519, L139
- Younes, G., Kouveliotou, C., van der Horst, A. J., et al. 2014, *ApJ*, 785, 52
- Younes, G., Kouveliotou, C., Jaodand, A., et al. 2017, *ApJ*, 847, 85